FarmFlow validation against full scale wind farms

E.T.G. Bot

August 2015
ECN-E--15-045

Acknowledgement

Abstract

For the accurate calculation of wind turbine wake effects in (large) offshore wind farms, ECN has developed the software tool FarmFlow. FarmFlow calculates the average velocities and turbulence intensities inside a wind farm. The wake model in FarmFlow is a 3D parabolised Navier-Stokes code, using a k-ε turbulence model to account for turbulent processes in the wake. A boundary layer model is used for the calculation of the free stream wind speed. For the deceleration and expansion of the near wake, FarmFlow uses an axisymmetric vortex wake model to calculate the stream wise pressure gradients, which are prescribed as a source term in the flow equations.

In various blind benchmark studies between 2009 and 2014, FarmFlow proved to provide the highest accuracy for large offshore wind farms in comparison with other wake models.

In the period 2012-2014 several modifications and improvements of FarmFlow have been applied for research projects within the FLOW program. These modifications and improvements are related to increased accuracy, increased computational speed, implementation of active wake control (AWC) using yaw misalignment, and extension of the boundary layer model to non-neutral conditions and extreme low turbulence levels.

A large amount of accurate experimental data from ECN Wind Turbine test station Wieringermeer (EWTW) has been used for the validation of FarmFlow, including all recent modifications. Additionally, experimental data from three large offshore wind farms have been compared with FarmFlow model results.

The calculated wake velocity deficits and turbulence intensities agree very well with experimental data for all wind speeds and ambient turbulence intensities, particularly for wake deficits and power performance at distances larger than 5 rotor diameters. When an extremely small turbine spacing is applied (i.e. less than 5 rotor diameters) FarmFlow overestimates the wake recovery. For large distances behind the rotor, FarmFlow tends to overestimate the generated turbulence intensity slightly. Comparisons with experimental data from the offshore wind farms Horns Rev and Nysted with a turbine spacing of 7 and 10 rotor diameters respectively have shown that wake losses of individual wind turbines are predicted very accurately.

Contents

Appendices

1
Introduction

For the accurate calculation of wind turbine wake effects in (large) offshore wind farms, ECN has developed the software tool FarmFlow. FarmFlow uses a wake model based on the UPMWAKE code [1]. This model is a 3D parabolised Navier-Stokes code, using a k-ε turbulence model to account for turbulent processes in the wake. The ambient flow is modelled in accordance with the method of Panofsky and Dutton [2]. The free stream wind as a function of height is calculated for a prescribed ambient turbulence intensity and the Monin-Obukhov length, which takes the atmospheric stability into account. For the deceleration and expansion of wind turbine wakes, FarmFlow uses an axisymmetric vortex wake model to calculate the stream wise pressure gradients, which are prescribed as a source term in the flow equations. This hybrid method of wake modelling in the near wake region, including an adapted near wake turbulence model, gives very accurate results in a very acceptable amount of computational time.

In various blind benchmark studies between 2009 and 2014, FarmFlow proved to provide the highest accuracy for large offshore wind farms in comparison with other wake models [13, 14].

In the period 2012-2014 several modifications and improvements of FarmFlow have been applied for research projects within the FLOW program. These modifications and improvements are related to increased accuracy, increased computational speed, implementation of active wake control (AWC) using yaw misalignment, and extension of the boundary layer model to non-neutral conditions and extreme low turbulence levels. In addition to the standard version with GUI, also a batch version for a windows cluster has been developed for studies on wind farm layout and power optimisation studies. The batch version produces the exact same output as the GUI-version. The GUI version has the benefits of easier composing input files, organizing wind farm data and post-processing calculated results. The batch version gives more freedom in using specific input in wind data, which is especially useful for simulation of wind farms using measured time series of wind data and for optimisation studies on wind farm layout and (active wake) control. All FarmFlow calculations have been done with the following version: FarmFlow 2.2.3, released on June 30, 2015.

In chapter 2 a short description of the FarmFlow program is given. Results of FarmFlow are compared with measurements in chapters 3 to 6. In chapter 3 experimental data

from the ECN Wind turbine Test station Wieringermeer (EWTW) is used for the validation of FarmFlow. In chapter 4 calculations on the Horns Rev offshore wind farm are compared with experimental results obtained from the EU FP7 project EERA DTOC [14]. In chapter 5, measurements of the Nysted offshore wind farm, obtained from the European Commission funded project "UpWind Wp8: Flow" [13], have been used for comparison with FarmFlow results. Calculations of the turbulence intensity with FarmFlow are compared with measurements at the Offshore Wind farm Egmond aan Zee (OWEZ) in chapter 6. Finally, the main conclusions are given in chapter 7.

2

FarmFlow

For the accurate calculation of wind turbine wake effects in (large) offshore wind farms, ECN has developed the software tool FarmFlow. The main graphical user interface of FarmFlow is shown in Figure 1.

Figure 1: Graphical user interface of FarmFlow.
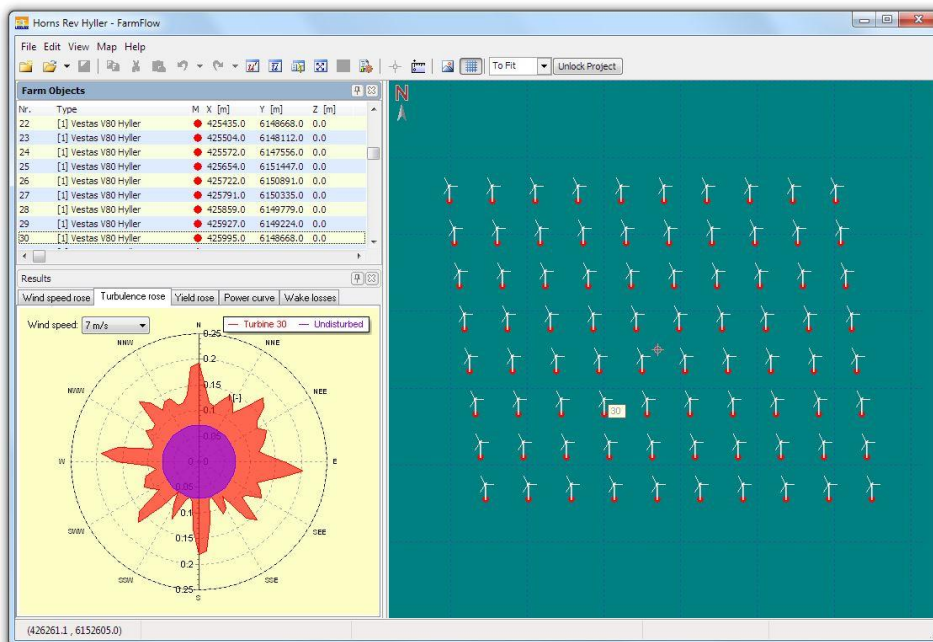
2.1 Wake model

The wake model in FarmFlow is based on the UPMWAKE code [1], originally developed by the Universidad Polytecnica de Madrid. UPMWAKE is a 3D parabolised Navier-Stokes code, using a k-ε turbulence model to account for turbulent processes in the wake. The ambient flow is modelled in accordance with the method of Panofsky and Dutton [2]. The free stream wind as a function of height is calculated for a prescribed ambient turbulence intensity and Monin-Obukhov length, which takes the atmospheric stability into account. The parameters of the k-ε turbulence model are adjusted such that the free stream turbulent kinetic energy matches the value from Panofsky and Dutton for neutral conditions.

In the original model, the wake is divided in a near wake region with a length of 2.25 rotor diameters (*D*), and a far wake region. Due to the parabolization, axial pressure gradients were neglected. Since the flow deceleration and wake expansion in the near wake are forced by axial pressure gradients, these effects could not be included in the original modelling, by which the turbulence modelling started at the far wake, using an initial empirical wake velocity profile at 2.25*D*.

The wake model has been improved in 2006 [7]. Thereto, the parabolization (and the subsequent enormous reduction in computational efficiency) was retained but the stream wise pressure gradient is not neglected anymore but prescribed as a source term in the flow equations. The stream wise pressure gradients are calculated via an inviscid, axisymmetric, free vortex wake method. The rotor is assumed to be a uniformly loaded actuator disc. From a prescribed thrust curve of the wind turbine the average axial induction is calculated according to BEM theory. The free vortex wake model then calculates the initial induced wake velocities that match the averaged axial velocity deficit in the rotor plane. With this method, the pressure gradients are a function of the axial force coefficient only. To save computational effort, the pressure gradients are calculated a priori for a large number of axial induction factors, so that the wake model only needs to interpolate the pressure gradients between the two nearest induction factors in this database. This hybrid method of wake modelling in the near wake region, including an adapted near wake turbulence model, gives very accurate results in an acceptable amount of computational time. For more detailed information on the wake modelling in FarmFlow, reference is made to [8].

2.2 Computational domain

The computational domain of the wake model in FarmFlow has the dimension of a rectangular box. The size of the grid cells has always been a compromise between accuracy and computational time. The size of the grid cells perpendicular to the flow direction is a fraction of the rotor diameter *D*. Until 2014, this has been D/15. From 2014, this size has been increased to D/9 while in flow direction the size has been increased with a factor 3. As a result, the computational speed has been reduced with a factor 20. The main drawback of a courser grid is a decrease of accuracy. However, in

the original model the effect of numerical diffusion has already been compensated by calibrating the k-ε turbulence model in the near wake region (see section 2.4). Therefore, a slight recalibration of the k-ε turbulence model in the near wake region could largely reduce the differences between the faster with the courser grid and original model.

The new computational domain of the FarmFlow wake model is shown in Figure 2. With a grid size of D/9 (perpendicular to the flow direction), the rotor area is covered by approximately 50 grid cells. In flow direction the grid begins at the rotor area with an exponentially increasing step size because of the slower wake development at larger distance downstream the rotor. At the rotor area the step size is 0.01D and after a distance of 15D, the maximum step size of 1.6D is reached.

Figure 2: 2D computational domain of FarmFlow. The drawing of the wind turbine is for indication of the rotor size only (rotor diameter is equal to 9 grid cells).
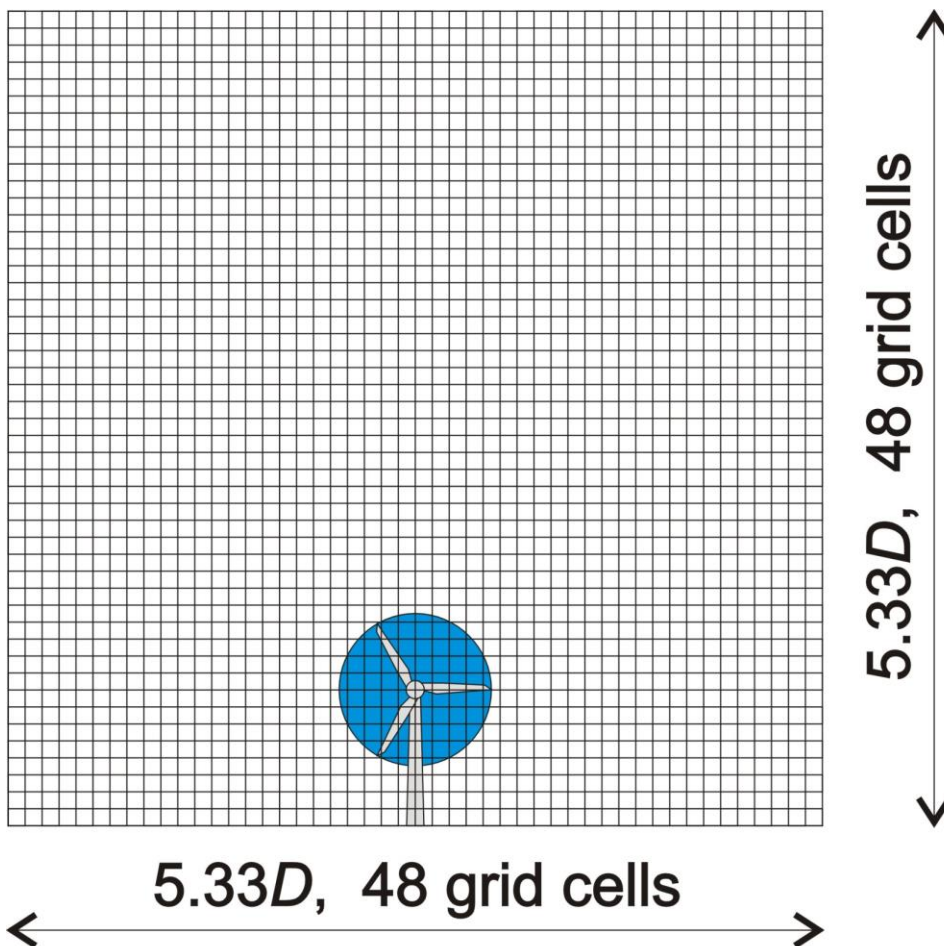
The dimensions of the computational domain are a compromise between acceptable computational effort accuracy of the results. Earlier test calculations with grid refinement [7] have shown that at least 13 nodes on the rotor diameter are necessary

for accurate results. With re-calibration of the turbulence model in the near wake, a reduction to 9 nodes turned out to be possible. Other test calculations have shown that dimensions of at least 5 rotor diameters are necessary for accurate results when arrays with more than 20 turbines are modelled.

For the top and bottom boundaries Dirichlet conditions are applied (i.e. zero perturbation is prescribed) while at the side boundaries Neumann conditions are applied.

The power production of wind turbines is based on the rotor average velocity calculated with FarmFlow and the power curve data. Because of the curved velocity profile, the rotor averaged velocity is slightly lower than the velocity at hub height. For this reason, the calculated power production of undisturbed wind turbines may be around 99% of the power curve. FarmFlow uses cubic splines with overshoot prevention to interpolate power and thrust values.

An example of the development of the calculated wind velocity in a long array of wind turbines with rotor diameter D = 126 m and a mutual distance of 6.8D is shown in Figure 3. The wake at 0.5D behind the first, the tenth and the twentieth turbine are shown. At the tenth turbine in the array, the boundary layer above the farm has been developed up to a height of approximately 5D. At the twentieth turbine, the axial velocity at 4D above the farm has been reduced with 1.0 m/s. The reduced amount of kinetic energy available in the flow above the wind farm decreases the potential wake recovery. Besides this effect, the size of wakes of neighbouring arrays will merge when the length of the arrays is long enough with respect to the distance between the arrays. As a result of the effect of reduced energy above the farm and the merging wakes of neighbouring arrays, a 'deep array effect' can be observed when the array length is larger than 10 turbines. For smaller arrays, the effect may be too small to be noticeable in measurements.

Figure 3: Calculated axial velocities at 0.5*D* behind the first, tenth and twentieth turbine in an array of turbines with rotor diameter *D* of 126 m and a mutual distance of 6.8*D*.
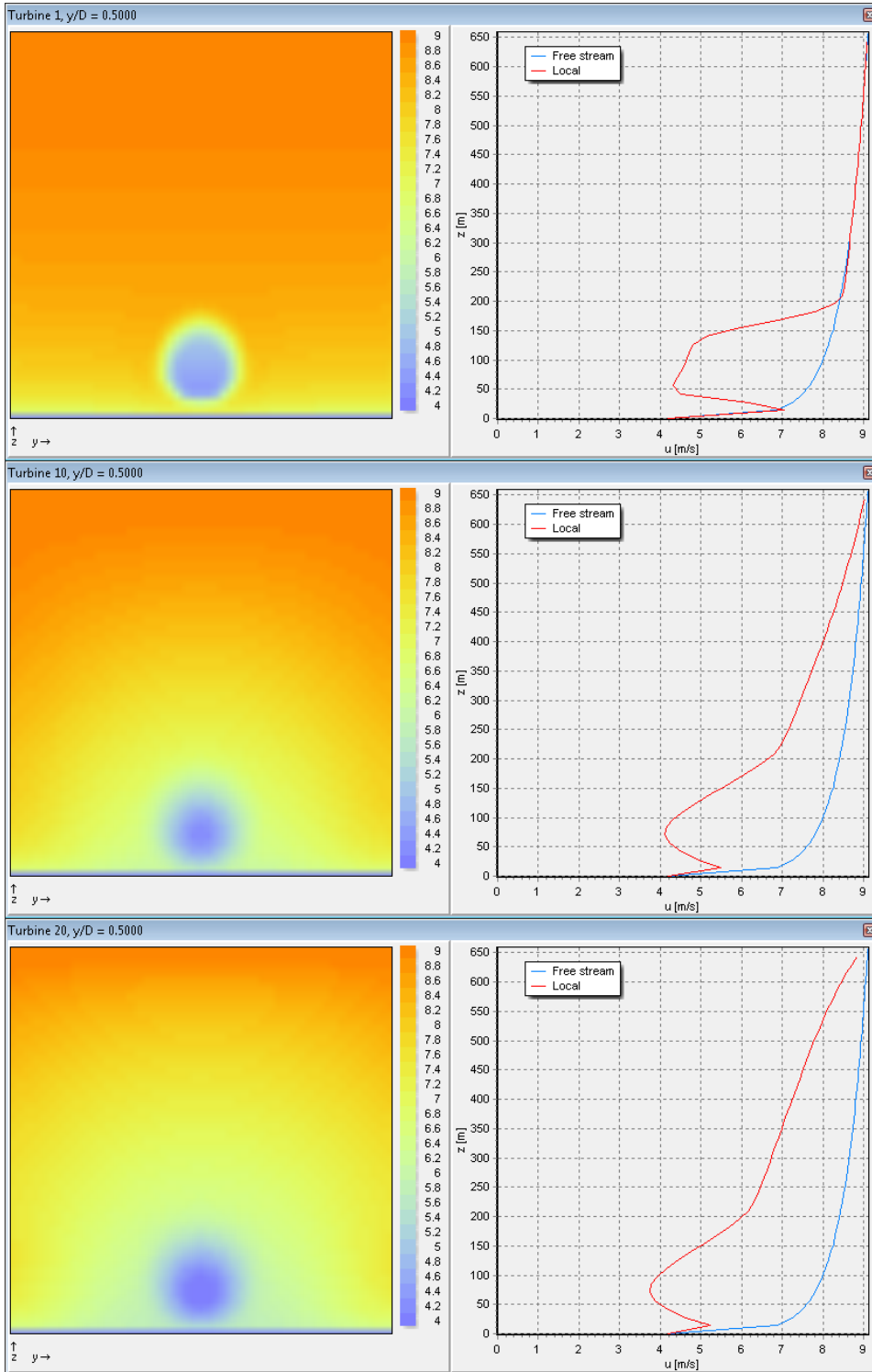
2.3 Wind direction uncertainty

In the atmosphere, the velocity and direction of the wind changes continuously. By using measured power curves based on 10 minute average samples, the effect of the continuous change of the wind on the power production is automatically accounted for. Unfortunately, this is not the case for the effect of wake losses in a wind farm. In a period of 10 minutes, wind directions change to values outside the wind direction bin in which the average result is stored. Due to these wind direction changes, the wake of a wind turbine rotor meanders laterally, which is not accounted for by the turbulence model. Fortunately, the effect of wake meandering on the annual yield of wind turbines is small, since both positive and negative effects of lateral wake meandering are cancelled out by each other. However, when field measurements averaged over small wind direction bins (< 15°) are compared with FarmFlow results, it is strongly recommended to correct the FarmFlow results for wind direction uncertainty to allow for fair comparison.

In this report, only 10 minute average values of measured wind direction are used for comparison with FarmFlow results. The full range of the continuous data of the wind directions is uncertain in these periods. For the validation of FarmFlow, a correction method is used to account for the full range of wind directions in 10 minutes average results. This correction method assumes a Gaussian probability distribution of the wind direction change in consecutive samples.

The standard deviation $\sigma_{\Delta\theta}$ of the wind direction change $\Delta\theta$ over consecutive sample periods is generally between 2.5° to 3.5° (according to measurements from the Horns Rev offshore wind farm and from the test wind farm EWTW). However, sometimes long periods occur in which the standard deviation is much smaller or much larger. If possible, it is always recommended to calculate the standard deviation of the wind direction from the measured consecutive samples:

$$\sigma_{\Delta\theta} = \sqrt{\frac{\sum_{i=1}^{n-1}(\theta_{i+1} - \theta_i)^2}{n-1}}$$

For best results it is important to reject data points for which $\theta_{i+1} - \theta_i > 3\sigma_{\Delta\theta}$. When time series are not available, a standard deviation of $\sigma_{\Delta\theta} = 3°$ is a reasonable value to use.

When the standard deviation of the wind direction change is known (or assumed), the correction for wind direction uncertainty can be applied by redistributing the calculated results over all wind direction bins, according to a Gaussian probability distribution of the wind direction change $\Delta\theta$ with standard deviation $\sigma_{\Delta\theta}$:

$$P_i(\theta_i) = \frac{1}{\sigma_{\Delta\theta}\sqrt{2\pi}} e^{-\frac{1}{2}\left(\frac{\theta_i - \theta_\mathrm{m}}{\sigma_{\Delta\theta}}\right)^2}$$

with θ_m as the wind direction of the original FarmFlow calculation. Applying this formula on the calculated results for wind direction θ_m actually spreads out the results

to all nearby wind direction bins θ_i according to a Gaussian distribution with the standard deviation $\sigma_{\Delta\theta}$, as plotted in Figure 4.

Figure 4: Gaussian probability distribution with a standard deviation of $\sigma_{\Delta\theta}$ = 3° for a wind direction bin size of 1° (left) and 5° (right).
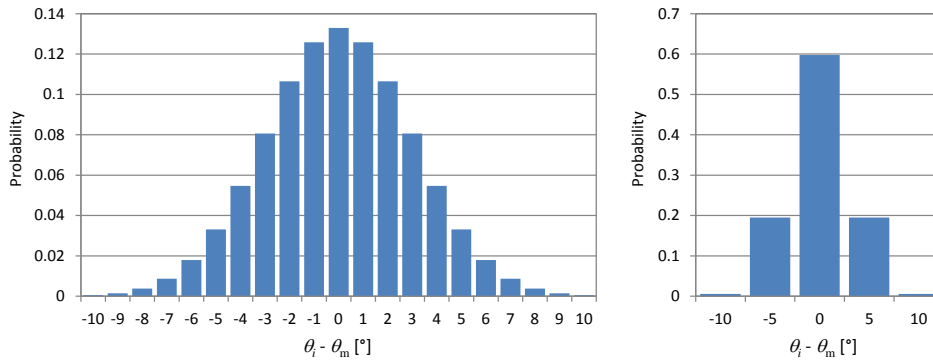
The above explained correction method does not take into account the fact that also wind turbines have trouble with wind direction uncertainty. Since the yaw angle is based on the average wind direction of a past period, turbines will operate with some yaw-misalignment most of the time. In this respect it is important to know that in the near wake region the deflection angle of the wake of a wind turbine with yaw misalignment is approximately 1.2 times larger than the yaw misalignment angle. The correction method for wind direction uncertainty on calculated power deficits in wind farms is therefore somewhat conservative.

2.4   Near wake turbulence modelling

The method of using prescribed pressure gradients made it possible to include the near wake region in the wake calculations, while still keeping the effort of a computational efficient parabolised code. However, results [8] with this new approach have shown that the deficit of the axial velocity at short distances behind the rotor is underestimated considerably with the standard k-ε model. The reason for this underestimated velocity deficit is a strong overestimation of the turbulence production in the shear layer of the wake. The overestimation of the turbulence production of the turbulence in the near wake region has probably two reasons. First, the k-ε model is an empirical model that needs to be recalibrated for different types of flow. The flow in the near wake region is very different from flow in the far wake region. Second, due to the coarseness of the computational grid, numerical diffusion occurs inside thin shear layer of the near wake region. To prevent numerical diffusion, the size of the grid cells need to be much smaller than the thickness of the shear layer. However, refining the grid will increase the computational time terribly and still not solve the problem of the different type of flows between the near wake region and the far wake region. Therefore, FarmFlow uses recalibrated k-ε model parameters in a region up to 3 rotor diameters

downstream the rotor in order to improve the prediction of turbulence production and velocity deficits.

According to the description of the wake behaviour from Crespo et al. [3], the wake of a wind turbine can be separated in three regions: a near wake region, a far wake region, and a transition region in-between. Figure 5 shows the development of the vertical velocity profile downstream a wind turbine. In flow direction the area is divided in four regions: the (undisturbed) free stream region upstream the rotor and the three wake regions. For each region a velocity profile is drawn in the picture. The near wake region ends approximately at two rotor diameters downstream the rotor, and the far wakes begins at approximately 4-5 rotor diameters downstream.

Figure 5: Development of the vertical velocity profile downstream a wind turbine.
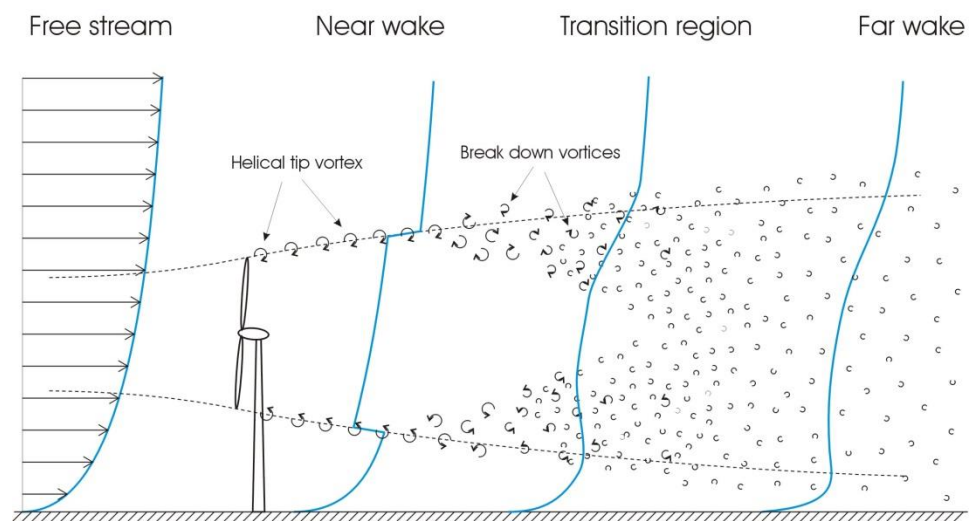
The near wake region starts at the rotor surface where wind energy is extracted by means of a pressure drop over the rotor plane. The cylindrical shear layer separates the slow moving air inside the wake from the air outside the wake. Inside the shear layer tip vortices, which are shed from the turbine blades, are following a helical trajectory. The velocity deficit inside the wake increases as a result of increasing pressure inside the wake, until this pressure reaches the pressure of the external flow. The wake expands as a result of the increasing velocity deficit. The stable system of helical vortices inside the shear layer produce only a small amount of turbulence. Because of limited turbulent diffusion inside the shear layer, the thickness of the shear layer grows slowly. PIV measurements [25] have shown that the effect of individual blades on axial velocity disappears beyond a distance of one rotor diameter, while the tip vortices stay present for a much longer time.

At the end of the near wake region, the tip vortices start to break down and produce high levels of turbulence. As a result of the increased turbulent diffusion, the shear layer thickness increases faster. When the shear layer reaches the wake axis, the near wake ends and the transition region begin. The transition region ends where the wake is completely developed with self-similar distribution profiles of the velocity deficit and

turbulence intensity. Here, in the far wake region, the wake meets the criteria for which the standard k-ε model has been calibrated.

For the near wake region and the transition region the standard k-ε model is not valid. Applying the standard k-ε model parameters will result in large overestimation of the turbulence production in the shear layer of the near wake region, which will then be spread over the whole wake area as a result of turbulent diffusion. Because of this, the recovery of the wake will start too soon and too fast. Kasmi and Masson [24] also noted this, and added an extra term to the transport equation for the turbulence energy dissipation rate. FarmFlow uses recalibrated k-ε model parameters for the near wake region and the transition region to correct the behaviour of the turbulence model. Only in the far wake region the standard k-ε model parameters are applied.

The target for the recalibration process of the k-ε model parameters has been to produce the best agreement with measurements in large offshore wind farms. For those wind farms, the distance between wind turbines are generally between 5 and 10 rotor diameters. Therefore, the aim of the recalibration process has been to get the highest accuracy of power prediction for wind turbine arrays with a turbine spacing of 5 to 10 rotor diameters. This automatically means that FarmFlow will still underestimate the wake deficits to some extent when a shorter turbine spacing than 5D is applied.

2.5 Active wake control

Active Wake Control (AWC) is a farm operation strategy that aims at improving the overall wind farm performance in terms of power production and/or turbine loads. Two concepts for AWC exist: reducing power and thrust of upstream turbines in favour of downstream turbines and applying yaw-misalignment of upstream turbines in order to steer the wake of these turbines away from downstream turbines. Implementation of the first concept is rather straightforward by applying different power and thrust curves. The implementation of the second concept is much more complicated and is described in this section.

A visualization of the AWC concept with yaw-misalignment is shown in Figure 6. The left hand side of this figure represents the normal situation without yaw-misalignment. The wake of the upstream turbine is visualized. The downstream turbine is operating in the right half side of that wake. A very important fact of this concept is that it is most beneficial when applied if the downstream turbine is positioned in only one half of the wake. The blue arrows visualize the flow in three cross-sections of the wake, and the purple arrows visualize the rotor induced flow that cause the velocity deficit.

Figure 6: Visualization of the Active Wake Control concept based on yaw-misalignment.
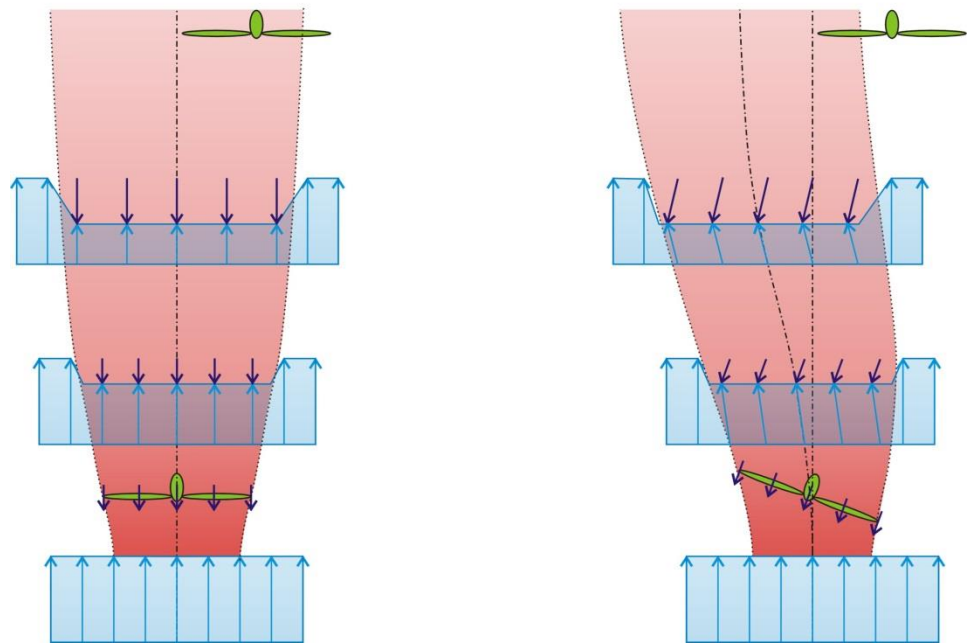
The right hand side of Figure 6 shows the same situation, except that the upstream turbine is misaligned with a yaw-angle $\gamma = 20°$. Because the induced flow of the rotor is directed normal to the rotor surface, the resultant flow field of the wake of the yawed turbine deflects from the wind direction. As a result, a much smaller part of the downwind turbine operates inside the wake of the upwind turbine.

The angle of the wake deflection depends on the thrust coefficient and the yaw angle. Since FarmFlow uses prescribed pressure gradients in the near wake region in order to induce the wake, i.e. the deceleration and expansion of the flow behind the rotor, implementation of yaw-misalignment is realized by prescribing these pressure gradients with respect to the yaw angle instead of the flow direction. Two empirical correction factors were used to optimize the wake deflection angle and wake deficit values. In addition, the width of the wake is reduced by a factor $\cos \gamma$.

Figure 7 shows comparisons of measurements from ECN's scaled wind farm and calculated wakes from FarmFlow for different yaw angles at a distance of 1.9D behind the rotor. The blue line shows the velocity deficit when the turbine has no yaw misalignment. For the red line the turbine has a fixed yaw angle of 237°, resulting in a yaw misalignment angle of 237°-WD. Therefore, only for a wind direction WD=237° there is no yaw misalignment for the red line so that its value is identical to the blue line. For the green line the turbine has a fixed yaw angle of 253°, resulting in a yaw misalignment angle of 253°-WD. Therefore, only for a wind direction WD=253° there is no yaw misalignment for the green line so that its value is identical to the blue line.

Figure 7: Wind speed deficits in the wake of a turbine for two fixed yaw angles (237° and 253°) and for a free yawing turbine (i.e. with no yaw misalignment) as a function of the wind direction.
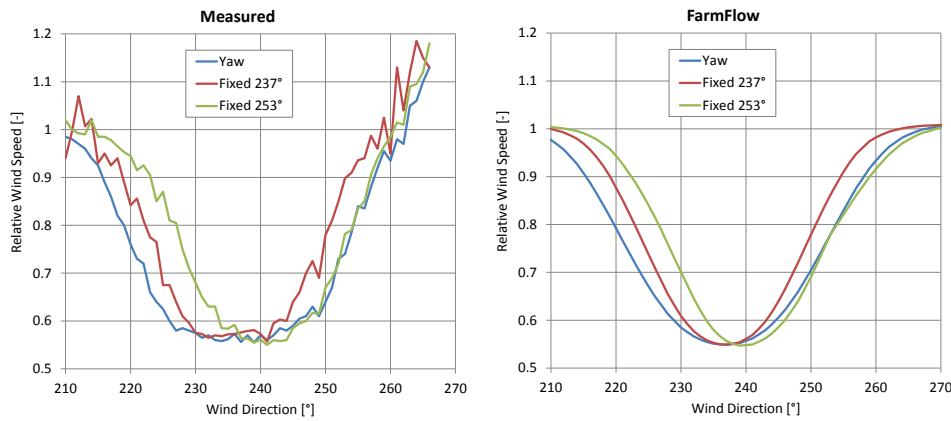
From these comparisons it can be concluded that FarmFlow predicts the velocity deficits in the wake of wind turbines with yaw misalignment quite well.

Yaw misalignment has a negative effect on the power production of concerning wind turbine. The mass flow through a wind turbine rotor decreases with a factor $\cos \gamma$ while it also changes the angle of attack of the rotor blades, leading to less efficient aerodynamic behaviour. As a result, the power of a yawed wind turbine below rated wind speed can be estimated with

$$P(\gamma) = P(0) \cos^{\beta} \gamma$$

When it is assumed that the yaw-misalignment has no effect on the aerodynamic behaviour of the rotor blades, the power reduces with the same factor as the reduction of the mass flow through the yawed rotor: $\cos \gamma$. On the other hand, when it is assumed that only the in-plane component of the wind inflow of a yawed rotor has no effect on the aerodynamic behaviour of the rotor, the power reduces with the same factor as the amount of kinetic energy that crosses the rotor area: $\cos^3 \gamma$. However, the in-plane component of the wind inflow does have a small positive effect on the pressure increase in front of the rotor, while yaw-misalignment does have an effect on the aerodynamic performance of the rotor blades. Therefore it is expected that the power coefficient must be in the range $1 < \beta < 3$. Wind tunnel measurements reported by Dahlberg and Medici [6] showed an average exponent of 2.48. An extensive database of field measurements analysed by Dahlberg [26] showed the exponent to vary between 1.8 and 5.5. Schepers [27] found a value of 1.8 based on measurements taken in the large DNW tunnel. In the NREL Phase VI experiment in the NASA-Ames wind tunnel a strong dependency of the exponent on the induction was found where at low induction the power was found to increase with yaw due to unsteady aerodynamic effects. Full scale tests on ECN's test site EWTW resulted in an average exponent of 2.1, and field test with a scaled wind farm resulted in an average exponent of 2.3. All these reported results indicate that there is a large uncertainty in the power exponent for yaw misalignment. In FarmFlow, a slightly conservative choice has been made with a power exponent of 2.3:

$$P(\gamma) = P(0) \cos^{2.3} \gamma$$

Figure 8 shows an example of the application of active wake control in FarmFlow on two turbines. As a function of wind direction, the optimized total power is found by applying yaw misalignment on the first turbine. When the wind direction is 0° (i.e. in line with the two turbines) the gain, shown by the green line and corresponding to the right axis, is negligible. The reduced power of the first turbine can be just compensated by the second turbine because of the wake deflection. When the wind direction is -8 to -5° or 5 to 8°, the gain of AWC is more than 6%. For these situations, the second turbine is positioned approximately in one half of the wake of the first turbine (like shown in Figure 6), which is most beneficial for active wake control. The results of Figure 8 are in very good agreement of the wind tunnel results of Dahlberg and Medici [6].

Figure 8: Example of optimized power output of two turbines with yaw misalignment in FarmFlow.
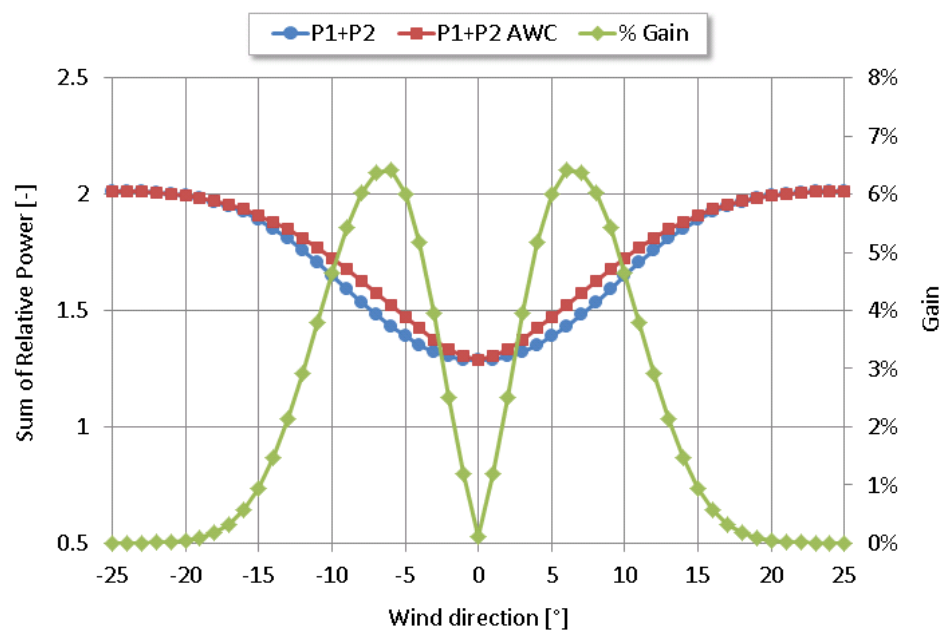
In comparison with the other strategy of AWC, i.e. reducing the thrust coefficient, there is a big difference in beneficial wind directions. When the thrust coefficient is reduced, the total wake effect is reduced so that the most beneficial wind direction is when the second turbine is in the centre of the wake. The strategy of applying yaw-misalignment does not reduce the total wake effect. Yaw-misalignment just causes deflection of the wake, which results in both areas of increased and areas of decreased velocity. Therefore, an explanation for the shape of the gain curve in Figure 8 can be found by examining the change of the velocity deficit when a turbine is yawed.

In Figure 9 the change of the velocity deficit at 3.7*D* behind a wind turbine is shown when the turbine is yawed at 20° (i.e. the difference of the velocity field is shown between yawed and non-yawed conditions). The left half of the wake region shows an increase of the velocity due to the yaw-misalignment, while the right half shows a decrease. As a result, a turbine positioned in the left part of a wake will produce more power when the first turbine is yawed in positive direction. When the turbine is

positioned in the right half of the wake, the first turbine needs to be yawed in negative direction. As a consequence, it is not beneficial to apply AWC when a turbine is in the centre of a wake. The most beneficial situation is when a turbine is approximately in one half of a wake.

Figure 9: Change of the velocity deficit at 3.7D behind a wind turbine when the rotor is yawed 20°.
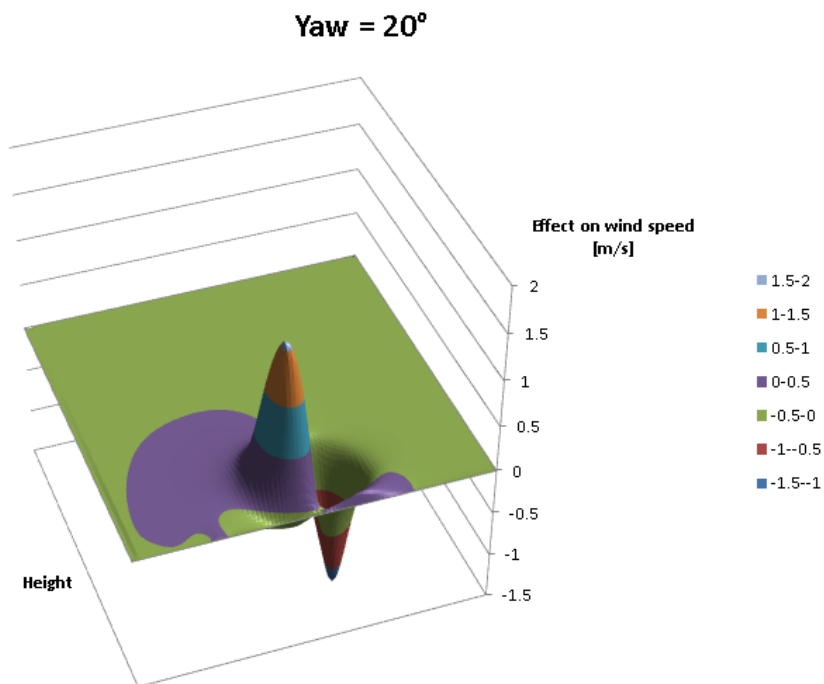
Because of the different beneficial wind directions of both strategies of AWC, both strategies can be applied in a wind farm in addition to each other, dependant on the wind direction.

3
EWTW

3.1   Farm layout

The ECN Wind turbine Test station Wieringermeer (EWTW) is located in the northeast of the province North-Holland, 35 km east of ECN Petten. In 2006, the test station comprised of 4 test locations for prototype wind turbines with two meteorological masts (three nowadays), and a test farm consisting of five 2.5MW wind turbines with another 108 meter high meteorological mast. Figure 10 shows the layout of the test farm.

The test locations for prototype wind turbines are numbered 1-4. The 5 variable speed and pitch regulated turbines of the test farm are numbered 5-9. The meteorological mast MM3 near the test farm (12) is located southeast from turbine 5 at 3.5 rotor diameters and southwest from turbine 6 at 2.5 rotor diameters distance. The test location and its surroundings are characterized by flat terrain, consisting of mainly agricultural area, with single farmhouses and rows of trees. The dike along the lake IJsselmeer is located at a distance of 925 m east of turbine 9. Two Neg Micon NM52 stall regulated wind turbines with a rotor diameter of 52 meter, numbered 13 and 14 in Figure 3.1, are located north of the test station. Number 13 is located northwest from turbine 5 at a distance of 1310 meter. It is important to note that the straight line through the rotor centre of turbine 13 and the meteorological mast intersects the rotor area of turbine 5, laterally only 13 meters from the rotor centre. The second NM52 wind turbine is located northeast of turbine 6 at a distance of 980 meter.

3.2   Turbine data

3.2.1 2.5MW test turbines

The turbine data for the five test turbines at the EWTW test farm are listed in Table 1. These variable speed, pitch controlled turbines have a rotor diameter and hub height of 80 m. The measured power curve and calculated thrust coefficients are taken from the Excel document 'PV_and_CDaxV.xls' [19], which was used for a large benchmark study

of wake models [13]. The measured power curve is shown in Figure 11. Figure 12 shows the calculated thrust coefficients together with the power coefficient as a function of the wind speed. It is remarkable that the measured thrust curve of this variable speed wind turbine shows no constant region in the thrust curve.

Table 1: Power and thrust data for the test turbines at EWTW.

Wind speed [m/s]	Power [kW]	Thrust coefficient [-]	Power coefficient [-]
4	26	0.8447	11.5
5	117	0.7982	12.1
6	251	0.7956	13.0
7	433	0.7939	14.1
8	669	0.7888	15.4
9	948	0.7438	16.5
10	1267	0.6878	16.4
11	1618	0.6512	16.8
12	1956	0.5766	17.0
13	2228	0.5083	17.0
14	2398	0.4239	17.0
15	2472	0.3297	17.0
16	2494	0.2654	17.0
17	2499	0.2184	17.0
18	2500	0.1828	17.0
19	2500	0.1550	17.0
20	2500	0.1330	17.0
21	2500	0.1152	17.0
22	2500	0.1007	17.0
23	2500	0.0886	17.0
24	2500	0.0786	17.0
25	2500	0.0701	17.0

Figure 11: Measured power curve of the 2.5MW test turbines at the EWTW test farm.
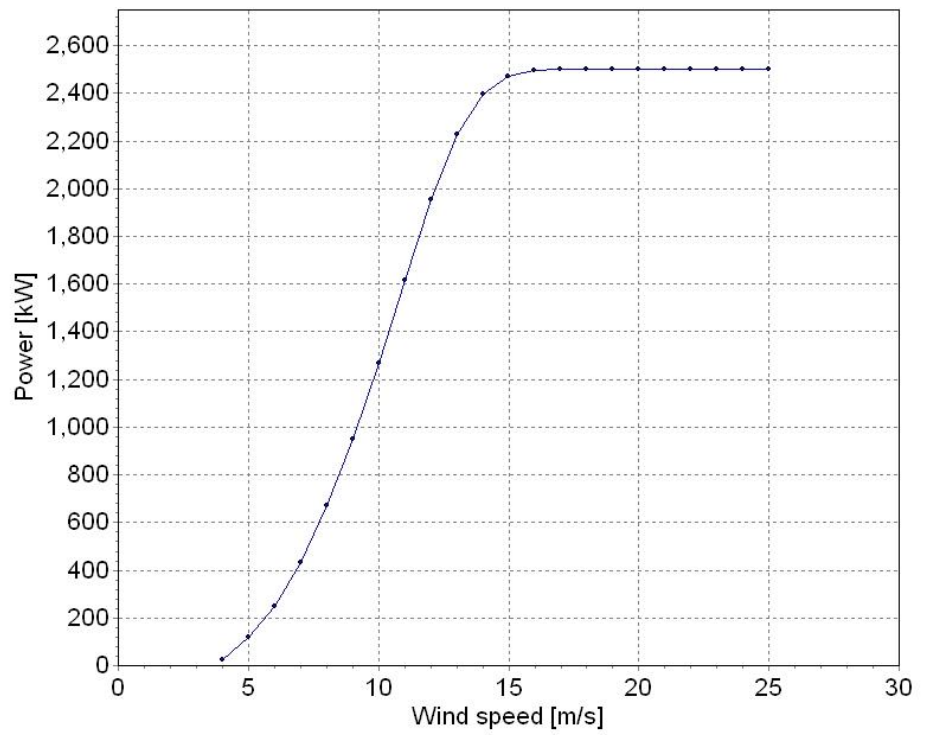
Figure 12: Calculated thrust curve and measured power coefficients of the test turbines.
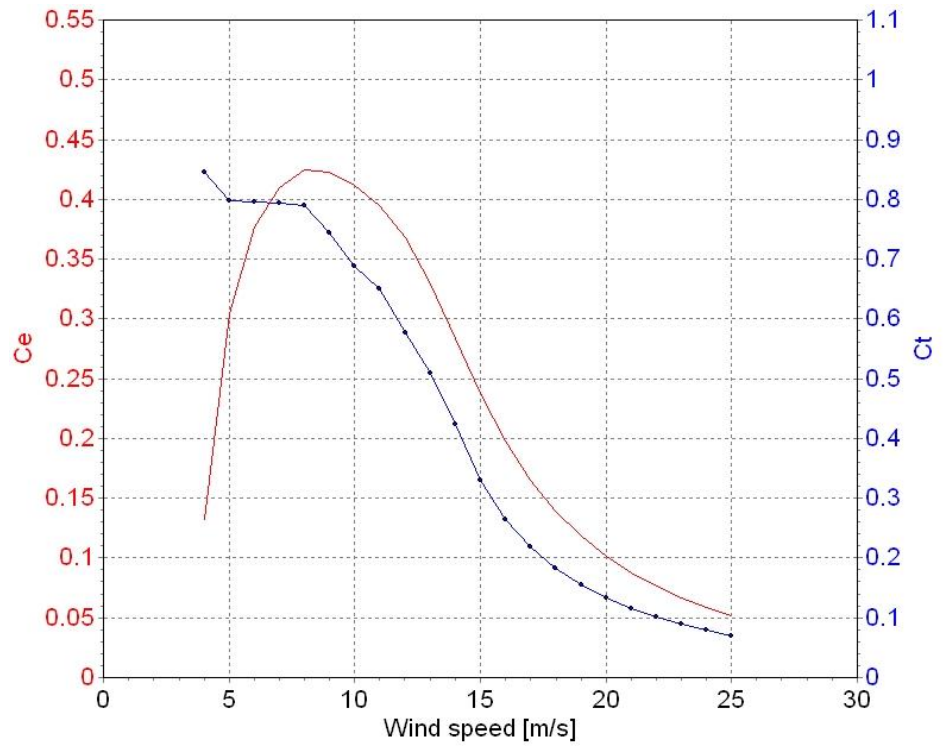
3.2.2 Neg Micon N52

The turbine data [20] for the Neg Micon NM52 wind turbines north of the test farm are listed in Table 2. The official power curve is also shown in Figure 13, and the official thrust curve together with the power coefficients are shown in Figure 14. These dual speed, stall controlled turbines have a rotor diameter of 52 m and a hub height of 49 m.

Table 2: Power and thrust data of the NM52 with 2 stall strips [20].

Wind speed [m/s]	Power [kW]	Thrust coefficient [-]	Power coefficient [-]
3	0.0	1.03	0.000
4	27.0	1.03	0.324
5	68.0	0.88	0.418
6	118.0	0.75	0.420
7	199.0	0.92	0.446
8	304.0	0.83	0.456
9	421.0	0.75	0.444
10	541.0	0.67	0.416
11	640.0	0.58	0.370
12	725.0	0.51	0.323
13	791.0	0.45	0.277
14	839.0	0.40	0.235
15	872.0	0.36	0.199
16	891.0	0.32	0.167
17	900.0	0.29	0.141
18	898.0	0.26	0.118
19	892.0	0.24	0.100
20	882.0	0.22	0.085
21	871.0	0.21	0.072
22	860.0	0.20	0.062
23	852.0	0.18	0.054
24	846.0	0.17	0.047
25	843.0	0.17	0.041

Figure 13: Official power curve of the Neg Micon NM52 wind turbine [20].
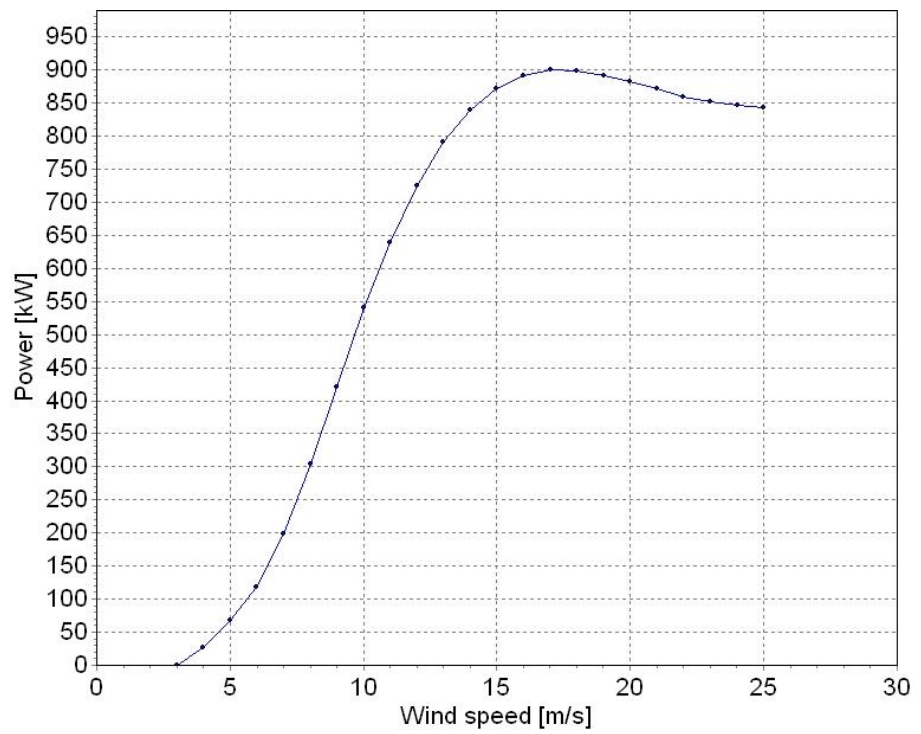
Figure 14: Official thrust curve and power coefficients of the NM52 [20].
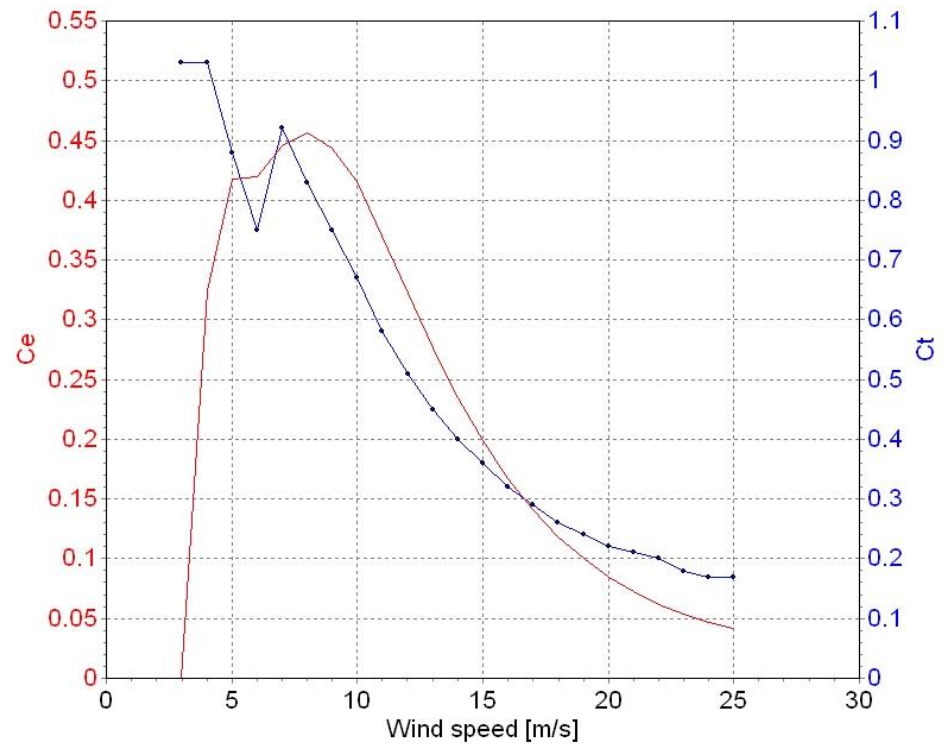
3.3 Ambient conditions

FarmFlow calculations are performed for wind speeds between 4 and 17 m/s with increments of 1 m/s, while the experimental data are often averaged results for larger wind speed intervals. Therefore, the model results are averaged over the same wind speed intervals as the experimental data. For accurate averaging of the model results, weighting factors derived from Weibull distributions of the ambient wind speed are used.

Table 3 presents the average wind speed at 80 m height. The data is taken from the EWTW meteorological database [9]. Because the original data is valid for a height of 71.6 m, the Weibull A values have been increased with a factor 1.011. An additional correction has been made for the sectors 60° and 300°. For these sectors, the measurements are disturbed by two wind turbines. To account for the effect of this disturbance on the annual wind speed, the Weibull A values of these two sectors have been increased with an additional factor 1.12, which was determined from FarmFlow calculations.

Table 3: Average wind speed at 80 m height between 2003 and 2007.

Sector [°]	Frequency [%]	Weibull A [m/s]	Weibull k	Wind speed [m/s]	Power density [W/m²]
0	6	6.9	2.2	6.11	247
30	6	7.3	2.2	6.47	292
60	7	7.9	2.2	7.00	370
90	8	8.1	2.9	7.22	334
120	6	7.6	2.5	6.74	299
150	5	7.3	2.7	6.49	254
180	9	8.1	3.0	7.23	329
210	13	8.7	2.2	7.71	493
240	13	9.3	1.9	8.26	697
270	11	8.0	1.9	7.10	445
300	9	7.4	1.7	6.61	407
330	8	7.4	2.1	6.56	317
All	101	8.0	2.3	7.11	407

The turbulence intensity at 80 m height is presented in Table 4. The data is arrived from measurements with the 3D sonic anemometer at 80 m height at the meteorological mast MM3 [12]. For wind directions where the measurements are disturbed by the test wind turbines, the data is interpolated with data from undisturbed wind directions. Additional plots of the wind data at 80 m height are shown in Figure 15.

Table 4: Annual average turbulence intensity at 80 m height.

Sector [°]	Turbulence intensity				
	4 m/s	6 m/s	8 m/s	10 m/s	12 m/s
0	0.115	0.108	0.106	0.106	0.107
30	0.090	0.085	0.083	0.083	0.085
60	0.082	0.077	0.076	0.076	0.078
90	0.078	0.073	0.072	0.072	0.074
120	0.082	0.077	0.076	0.076	0.078
150	0.090	0.085	0.083	0.083	0.084
180	0.100	0.095	0.093	0.093	0.093
210	0.105	0.100	0.100	0.100	0.100
240	0.105	0.100	0.100	0.100	0.100
270	0.105	0.100	0.100	0.100	0.100
300	0.105	0.100	0.100	0.100	0.100
330	0.110	0.105	0.105	0.105	0.105
All	0.105	0.099	0.098	0.098	0.099

Figure 15: Wind data plots for EWTW at 80 m height.

28
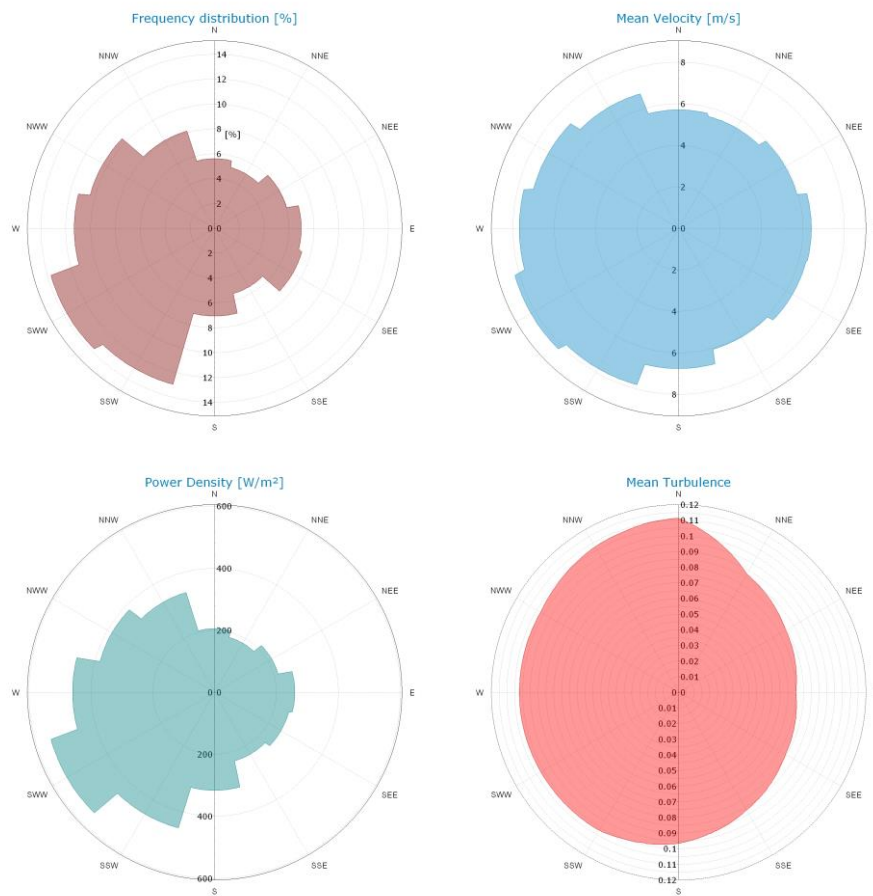
3.4 Results

3.4.1 Turbine performance

In Figure 16, Figure 17, and Figure 18 the calculated performance of the turbines are compared with measurements for wind directions between 230 and 320° and wind speeds of 4 to 6, 6 to 8 and 8 to 10 m/s. The width of the calculated wake profiles agrees very well with the measurements for all wind speeds. For the wind speed range 4-6 m/s also the calculated maximum wake effect shows very good agreement with the measurements. For higher wind speeds, the maximum wake effect is underestimated. This underestimation of the wake effects was expected, since the turbulence model in the near wake region has been calibrated for wind turbine arrays with a turbine spacing of $5D$ or larger, while the 5 test turbines at EWTW have a turbine spacing of only $3.8D$.

The calculated wake effect clearly decreases with increasing wind speed, while the measured wake effects are almost constant with wind speed. Considering the power and thrust coefficients of these turbines, the FarmFlow results seem to be more obvious. According to Figure 12, the trust curve is nearly constant between 5 and 9 m/s while the power coefficient shows a strong increase between 4 and 7 m/s. The wind speed at the turbines operating in full wake are approximately 80% of the free wind speed. This means that the power coefficient for turbines in full wake at a free wind speed of 5 or 6 m/s drops significantly, while at higher free wind speeds, the turbines in full wake operate at nearly the same power coefficient as turbine 5.

Figure 16: Relative performance compared to turbine 5 for wind speeds between 4 and 6 m/s.
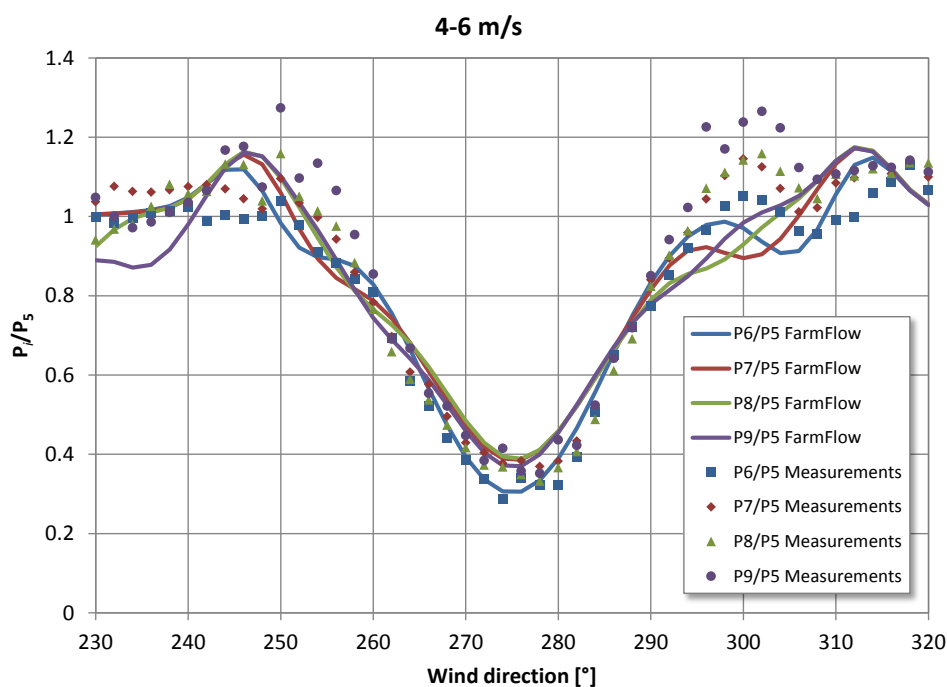
Figure 17: Relative performance compared to turbine 5 for wind speeds between 6 and 8 m/s.
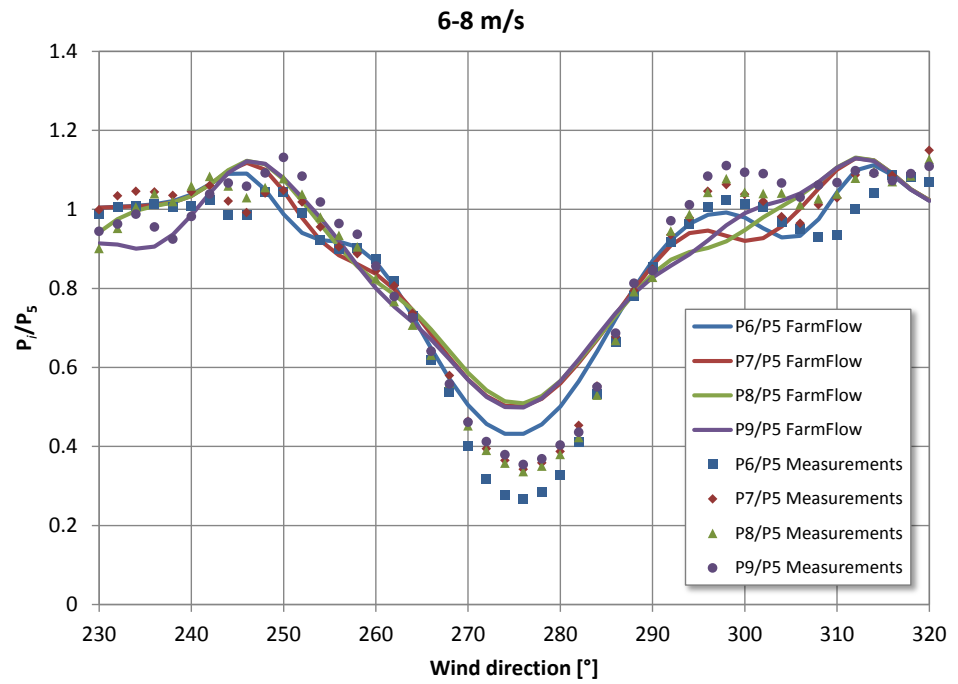
Figure 18: Relative performance compared to turbine 5 for wind speeds between 8 and 10 m/s.
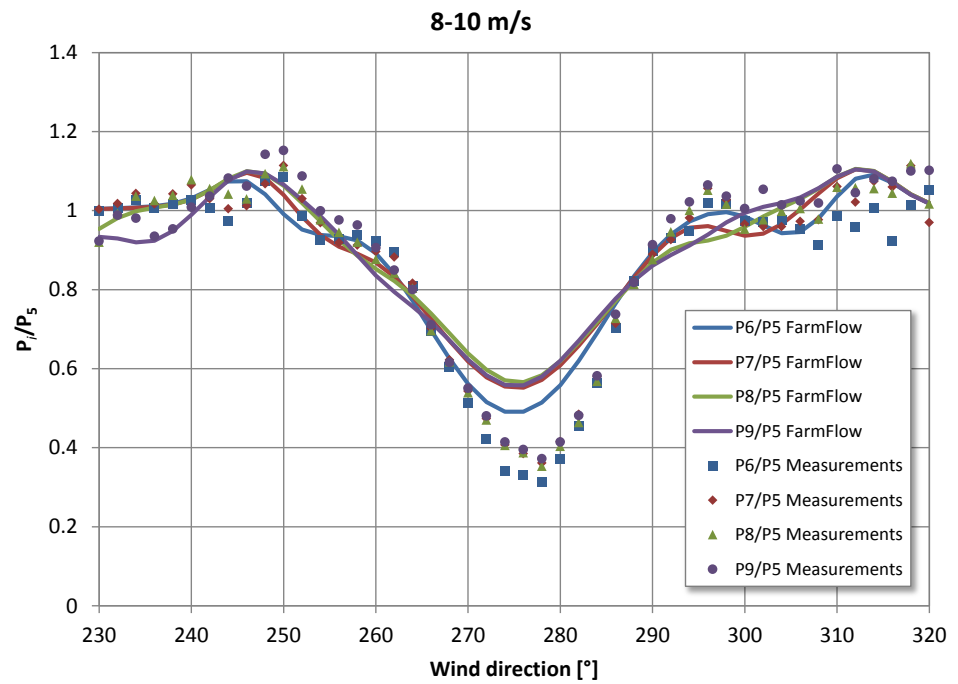
These different levels of wake effects between smaller and higher wind speeds in the FarmFlow results are definitely caused by the steep power coefficient curve. It is therefore not clear why this effect is not seen in the measurements.

The maximum performance reduction occurs at 275°, when the wind turbine row is parallel to the wind direction. Figure 19 shows the calculated and measured relative performance for this wind direction. The results are Weibull averaged for wind speeds between 4 and 10 m/s. Whereas the shape of the curve is predicted very well by FarmFlow, the average power reduction in full wake is underestimated with 22%. This underestimation is consistent with the results at higher wind speeds of Figure 18. Note that higher wind speeds have a stronger influence on the average results because of the much higher power production.

As mentioned, the prediction of higher power in full wake conditions for the EWTW test turbines was expected from the fact that the near wake turbulence model is calibrated for distances between 5 and 10D, while the spacing of the turbines is only 3.8D.

Figure 19: Relative performance in full wake compared to the first turbine in the row. Results are Weibull averaged for wind speeds between 4 and 10 m/s.
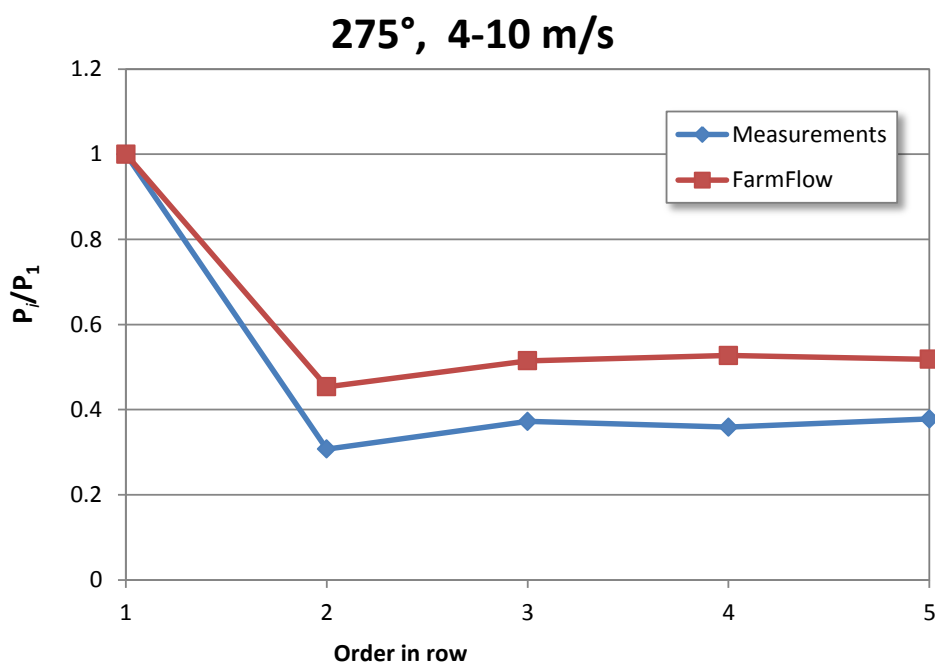
3.4.2 Velocity deficits and turbulence at met mast MM3

Figure 20 shows the measured and calculated average velocity deficits at the meteorological mast MM3 at 80 m height. The measured and calculated average

turbulence intensity are shown in Figure 21. The calculations are performed for ambient wind speeds between 5 and 15 m/s, and averaged according to the Weibull data of section 3.3. The ambient wind speed is determined from the nacelle anemometer of turbine 5, which has been calibrated at free wind conditions.

Figure 20: Relative wind speed at MM3 with respect to the wind speed at turbine 5. At 95° turbine 5 operates in the wakes of turbines 6 to 9.
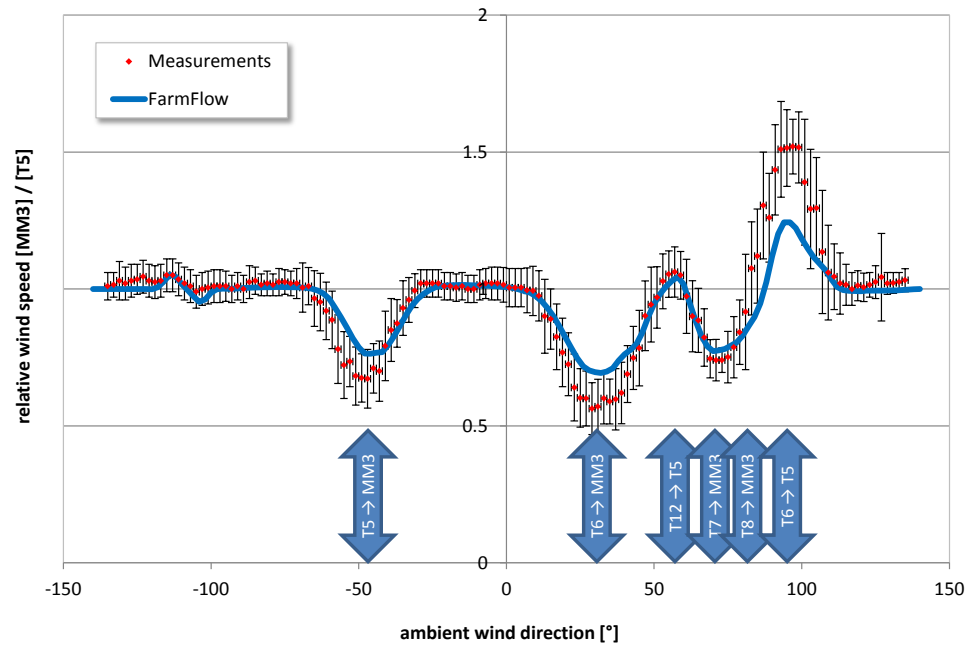
When MM3 is in the wake of T5 (-46°) or in the wake of T6 (30°), FarmFlow underestimates the wind speed deficit. When MM3 is in the wake of T7 (70°), T8 (80°) or T9 (85°), the wind speed calculated with FarmFlow agrees very well with the measurements. The only difference between T5 and T6 compared to T7, T8 and T9 in these measurements are the distance of these turbines with respect to MM3. This result shows clearly that FarmFlow underestimates the wake deficit only at distances less than 5 rotor diameters. The measured wake deficits of turbines T5 (3.5D) and T6 (2.5D) are underestimated, while the wake deficits of turbines T7 (5.4D), T8 (9D) and T9 (12.8D) agree very well with the measurements.

At a wind direction of 95°, an increase of the relative wind speed is shown in Figure 20. This is because the 'undisturbed' wind speed is measured with the nacelle anemometer of turbine T5, while this turbine operates in the full wake of turbines 6 to 9 at this wind speed. Because of the small distance between the turbines, the increased wind speed at 95° is underestimated by FarmFlow.

Figure 21 shows that the calculated turbulence intensities are of the same level as the measurements. The turbulence intensity is here defined as $I = \frac{\sigma[\text{MM3}]}{U[\text{T5}]}$, i.e. the standard deviation of the measured wind speed at the meteorological mast is divided by the wind velocity measured with the nacelle anemometer of turbine 5. Except for wind

directions between 80° and 115° the measured wind velocity at turbine 5 is undisturbed.

Figure 21: Average turbulence intensity $I = \frac{\sigma[\text{MM3}]}{U[\text{T5}]}$
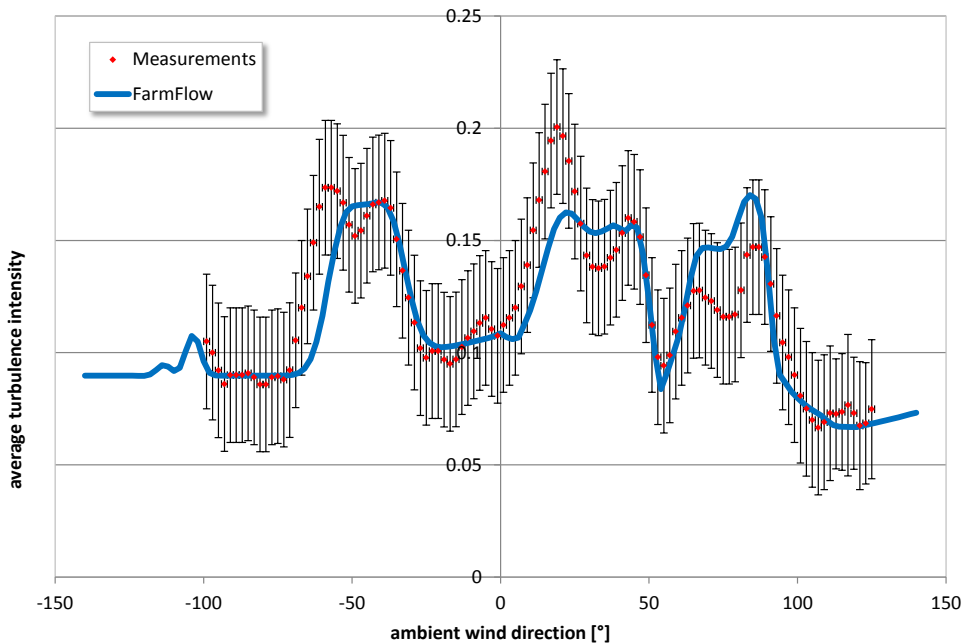
In general terms, the calculated wake effects agree very well with the measurements when the measurement position from the wind turbines is at least 5 rotor diameters. For distances less than 5D, the velocities in the wake are underestimated.

It should be noted that the effect of turbulence on power performance is not modelled in FarmFlow. The power curve is normally valid for a maximum turbulence intensity of 10%. According to the measurements, the turbulence intensity is between 15 and 20% in the full wake of wind turbines when the distance tor the rotor is smaller than 5D.

In Figure 22 the calculated performance is compared with measurements as a function of the ambient turbulence intensity for an ambient wind speed of 7 m/s at hub height. The shape of the calculated curves agree very well with the experimental data. At turbulent intensities below 12%, there is a clear difference between the power performance of the 2nd (T6) and last (T9) turbine in the row. For higher turbulence intensities, the performance of 4 turbines T6 – T9 are more similar. The FarmFlow results show the same trend, with only an underestimation of the wake losses due to the small distance between the turbines.

Figure 22: Measured (left) and calculated (right) minimum performance for different positions in a row as a function of the ambient turbulence intensity and at an ambient wind speed of 7 m/s at hub height.
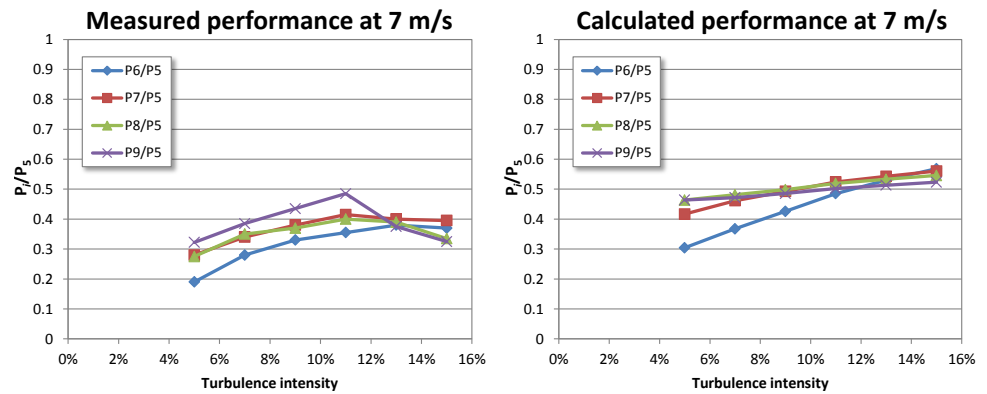
In Figure 23 the calculated performance is compared with measurements as a function of the ambient wind speed for all turbulence intensity classes. At 5 m/s wind speed the calculated performance agrees very well with the measurements. For higher wind speeds, the calculated power reduction is underestimated. When all results are averaged with the Weibull probability curve, the total power production calculated with FarmFlow is overestimated with 14.5%. These results are comparable with the results of Figure 16 – Figure 19. Again, it is not clear why the measurements show no influence of wind speed between 5 and 8 m/s on the power reduction in full wake operation. It is however perfectly clear why the FarmFlow calculations show a strong increase of the power performance in the same wind speed range: the combination of a flat thrust curve and a very steep power coefficient curve in this wind speed range. Therefore, the calculated curve seems to be the more logical outcome in this comparison.

Figure 23: Measured (left) and calculated (right) minimum performance for different positions in a row as a function of the ambient wind speed at hub height.
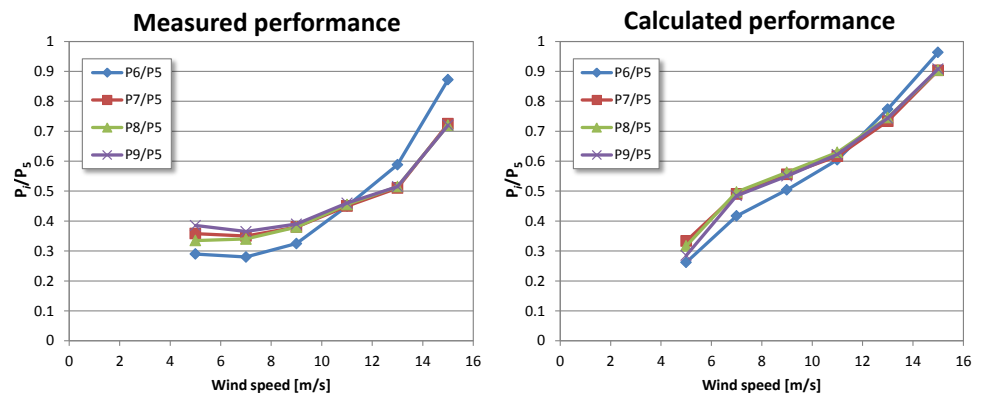
4

Horns Rev

4.1   Farm layout

The Horns Rev offshore wind farm with a capacity of 160 MW consists of 80 Vestas V80 2.0MW wind turbines [13]. It is located 15 km west of Blåvandshuk at the west coast of Jutland, Denmark.

Figure 24: Layout of the Horns Rev wind farm.
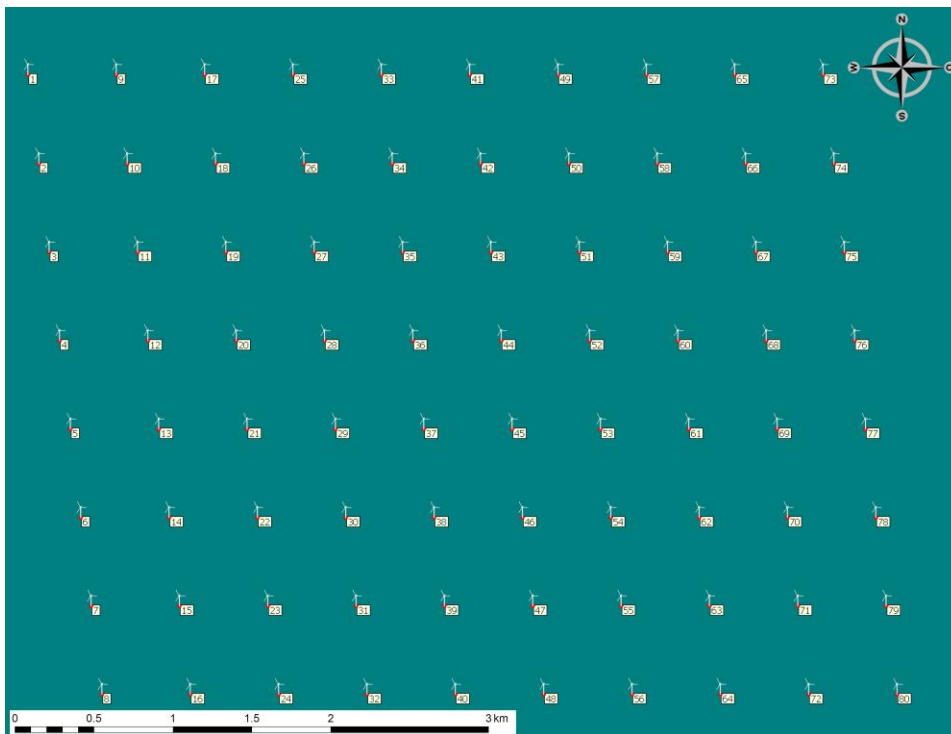
The pitch controlled wind turbines with rotor diameters of 80 m and hub heights of 70 m above sea level are aligned in 8 rows of 10 turbines, as indicated in Figure 24. The angle between the rows and columns is approximately 83.15°. The turbine spacing both in rows and in columns is 7 rotor diameters (560 m).

4.2 Turbine data

The turbine data for the Vestas V80 are listed in Table 5. These turbines have rotor diameters of 80 m and hub heights of 70 m above mean sea level (MSL). The official power curve [13] is shown in Figure 25, and the thrust curve and power coefficients are shown in Figure 26. As the Vestas V80 is a pitch controlled variable speed wind turbine with constant tip speed ratio and pitch angle at low to medium wind speeds, the thrust coefficient is almost constant up to 10 m/s.

Table 5: Vestas V80 power and thrust data [13].

Wind speed [m/s]	Power [kW]	Thrust coefficient [-]	Power coefficient [-]
4	66.6	0.818	0.338
5	154.0	0.806	0.400
6	282.0	0.804	0.424
7	460.0	0.805	0.436
8	696.0	0.806	0.442
9	996.0	0.807	0.444
10	1341.0	0.793	0.436
11	1661.0	0.739	0.405
12	1866.0	0.709	0.351
13	1958.0	0.409	0.289
14	1988.0	0.314	0.235
15	1997.0	0.249	0.192
16	1999.0	0.202	0.159
17	2000.0	0.167	0.132
18	2000.0	0.140	0.111
19	2000.0	0.119	0.095
20	2000.0	0.102	0.081
21	2000.0	0.088	0.070
22	2000.0	0.077	0.061
23	2000.0	0.067	0.053
24	2000.0	0.060	0.047
25	2000.0	0.053	0.042

Figure 25: Power curve of the Vestas V80 wind turbine.
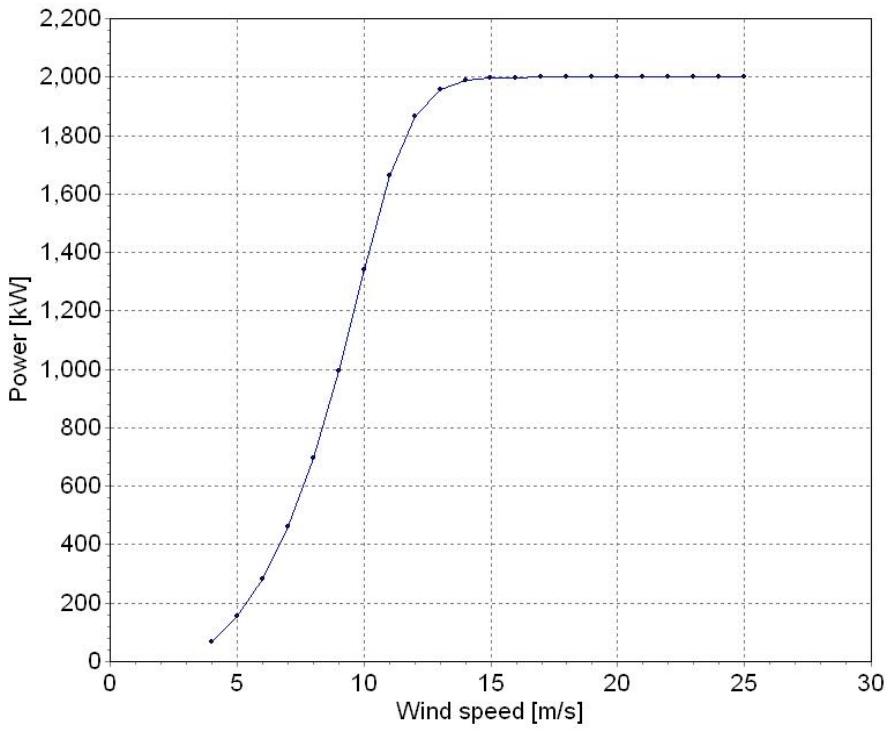
Figure 26: Power and thrust coefficients of the Vestas V80 wind turbine.
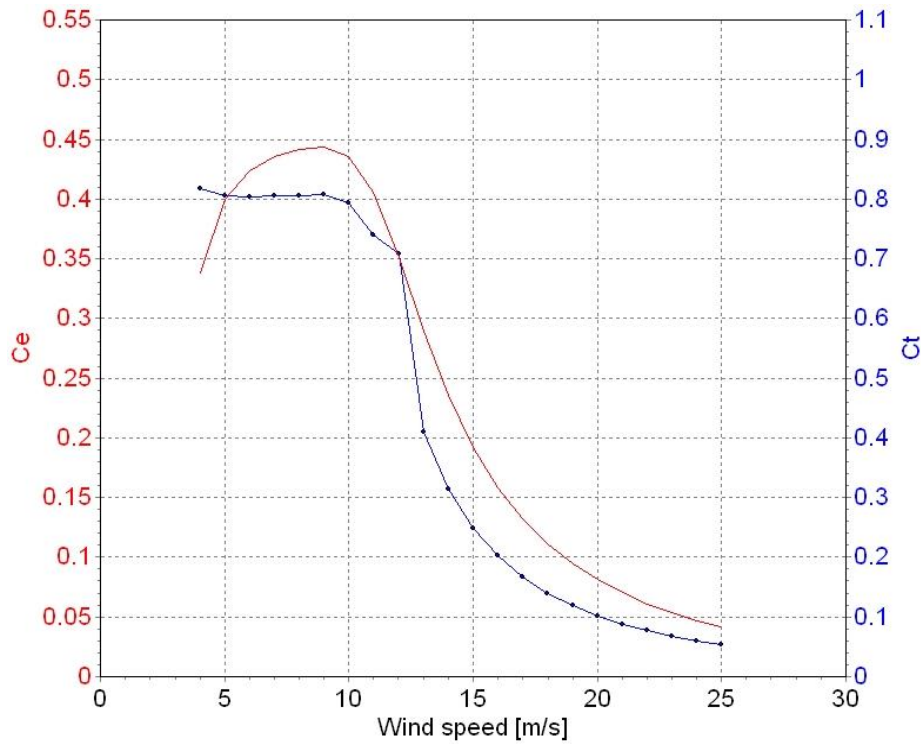
4.3 Ambient conditions

The power of all turbines have been recorded during a period of 17 hours where the wind direction has been along the rows and the wind speed has been varying between 6 and 10 m/s. The ambient wind speed and wind direction have been derived from calibrated nacelle anemometer measurements on wind turbine 7, which has an undisturbed inflow for all measured wind directions. The turbulence values for each wind sector and wind speed are listed in Table 6. The turbulence data are derived from anemometer recordings of a meteorological mast at 62 m height above MSL, 13 km north of turbine 1.

Table 6: Turbulence values at 62 m height above MSL.

Wind direction [°]	6 m/s [%]	8 m/s [%]	10 m/s [%]
255	7.2	6.6	6.0
260	7.0	6.5	6.4
265	7.7	7.1	6.8
270	7.2	6.9	7.5
275	7.7	6.9	6.9
280	8.2	7.4	7.5
285	8.2	7.2	7.4

Figure 27 shows the measured time series of the wind speed and nacelle position of turbine 7 on basis of 10 minute averaged data. The wind speed has been varying between 6 and 10 m/s. The data for wind speeds below 7 m/s are most limited: only 2.5 hours have been recorded, while the wind direction changed almost continuously from 265° to 290°. For wind speeds below 7 m/s it takes more than 15 minutes before the wakes of the turbines in the first column arrive at the last turbines in the last column. Because the traveling speed of the wakes is slower than the undisturbed wind speed, the wind direction uncertainty of 10 minute average samples may be quite large. To be conscious of this problem, comparisons are made for different wind direction sectors of 5°, 15° and 30° wide.

4.4 Results

Figure 28 shows the normalized power deficit of turbine 15, operating in the single wake of turbine 7 (see Figure 24) as a function of the wind direction for ambient wind speeds between 7 and 9 m/s at 62 m above MSL [15]. The included error bars are represented by the standard deviation of 5° sectors. This means these error bars do not represent standard error values, since the standard deviation is not divided by the square root of the (unknown) number of samples.

For the FarmFlow results, a fitted standard deviation of the wind direction change $\sigma_{\Delta\theta} = 3.64°$ has been used. With this value, both the wake width and the maximum deficit show good agreement with the measurements. At both sides of the wake, the measured curve shows only positive values between 0.01 and 0.03, which might indicate that the reference turbine 7 performs about 2% better than turbine 15.

Figure 29, Figure 30, and Figure 31 show normalized power deficits for a wind direction of 270° and wind direction bin size of 5°, 15° and 30° respectively. During these measurements the turbines 1 to 8 (first column of the farm) have an undisturbed inflow. Turbine 7 is used as reference turbine for the normalization of the power deficits. For the FarmFlow calculations, the standard recommended value for the standard deviation of the wind direction change $\sigma_{\Delta\theta} = 3.0°$ has been used to post process the results.

Figure 28: Normalized power deficit of wind turbine 15 (see Figure 24) as a function of the wind direction for ambient wind speeds between 7 and 9 m/s at 62 m above MSL.

Single wake power deficit; $7 < V_{62} < 9$ m/s
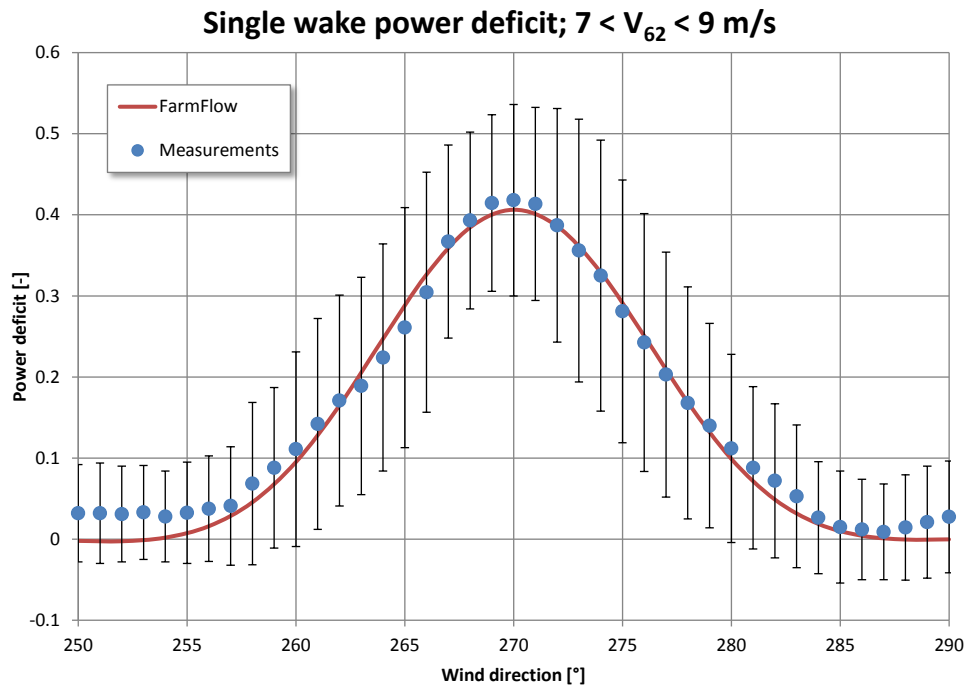
Figure 29: Normalized power as a function of column number in the Horns Rev wind farm for ambient wind speeds between 7.5 and 8. 5 m/s and wind directions of 270 ± 2.5°.

WD: 270 ± 2.5°
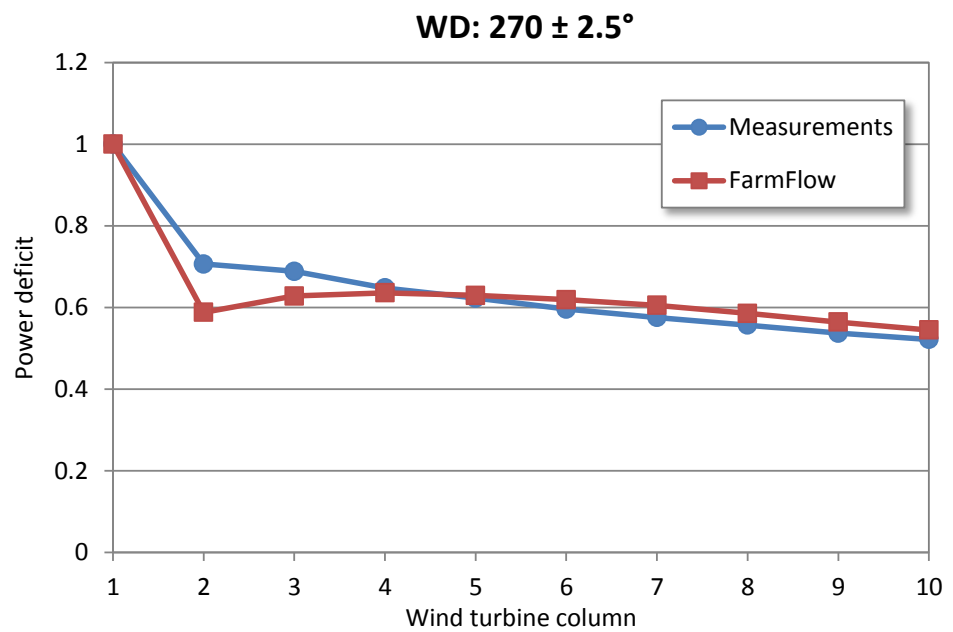
Figure 30: Normalized power as a function of column number in the Horns Rev wind farm for ambient wind speeds between 7.5 and 8. 5 m/s and wind directions of 270 ± 7.5°.

WD: 270 ± 7.5°
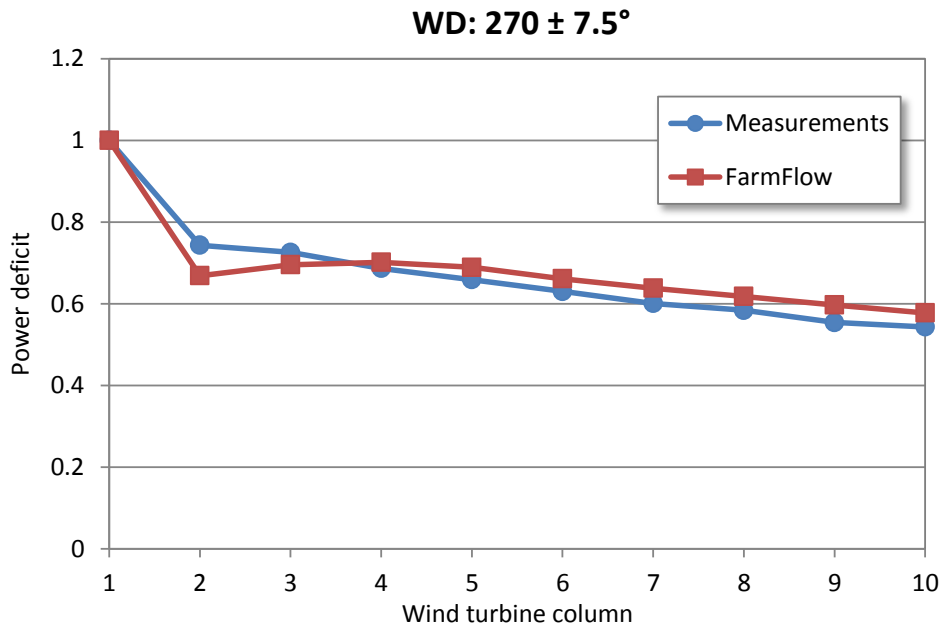
Figure 31: Normalized power as a function of column number in the Horns Rev wind farm for ambient wind speeds between 7.5 and 8. 5 m/s and wind directions of 270 ± 15°.

WD: 270 ± 15°
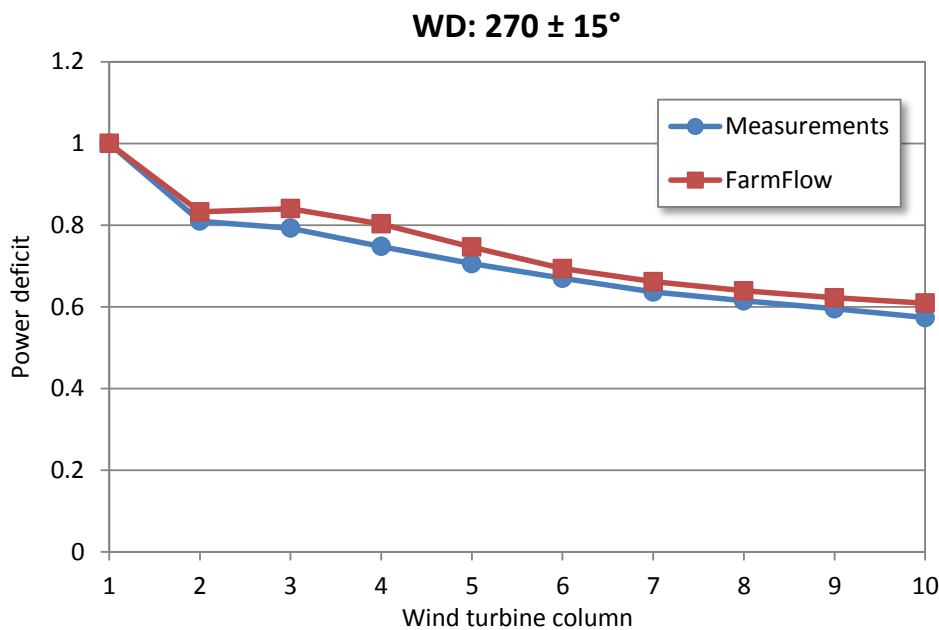
Except for the second column (single wakes with small wind direction bins) in Figure 29, the calculated power deficits agree very well with the measurements. For the single

wakes in the second column, FarmFlow calculates a maximum power deficit of approximately 40%, which agrees very well with the power deficit of Figure 28. For unknown reasons however, the measurements of the single wake power deficits in Figure 29 show much lower power deficits of approximately 41%.

A comparison of the total power deficit for all three wind direction bins is given in Table 7. The total power deficit is overestimated with only 0.5% for the smallest bin size of 5°, and underestimated with only 1.2 and 3.0% for the bin sizes of 15° and 30° respectively.

Table 7: Total power deficit for different wind direction bin sizes.

Bin size [°]	Measured deficit [%]	Calculated deficit [%]	Difference [%]
5	35.5	36.0	0.5
15	32.7	31.5	-1.2
30	28.5	25.5	-3.0

5
Nysted

5.1　Farm layout

The Nysted offshore wind farm is located south of Lolland, Denmark, and consists of 72 Bonus B82/2300 wind turbines with a total capacity of 165.6 MW. These 2.3 MW active stall controlled wind turbines have rotor diameters of 82.4 m and hub heights of 68.8 m above mean sea level (MSL). The turbines are aligned in 8 rows of 9 turbines [13], forming a parallelogram as indicated in Figure 32. The turbine spacing is $5.85D$ (482 m) from north to south, and $10.5D$ (867 m) from east to west. The angle between the rows and columns is 80.1°. Two downwind meteorological masts (numbers 75 and 76) are located at distances of 2 and 6 km, aligned with the middle row of turbines.

Figure 32: Layout of the Nysted wind farm.
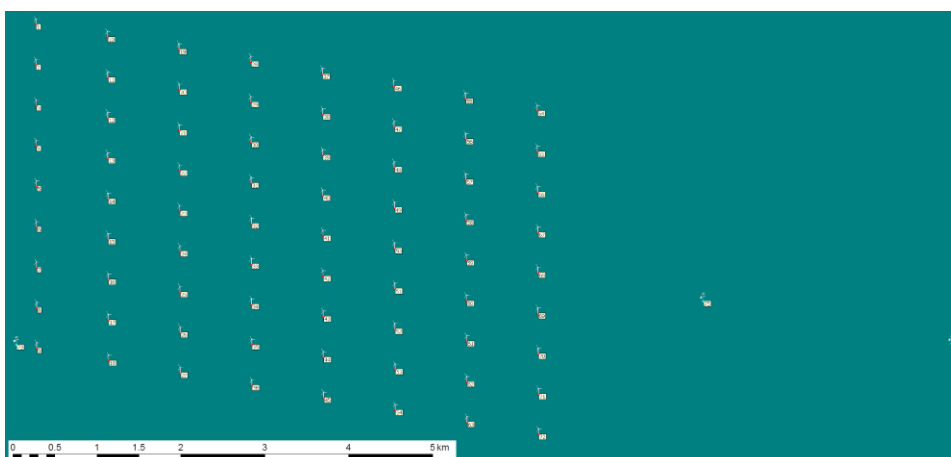
5.2 Turbine data

The turbine data for the Bonus B82/2300 are listed in Table 8. These turbines have rotor diameters of 82.4 m and hub heights of 68 m above MSL. The official power curve [18] is shown in Figure 33, and the thrust curve and power coefficients are shown in Figure 34. As the Bonus B82/2300 is a dual speed wind turbine, running with constant tip speed ratio and pitch angle at low to medium wind speeds, the thrust coefficient shows a discontinuity between 6 and 7 m/s. The thrust coefficients above rated wind speed are much too low for an active stall turbine and are probably based on an active pitch-to-vane controlled wind turbine. Fortunately, only values below rated wind speed are used here for validation of FarmFlow.

Table 8: Bonus B82/2300 power and thrust data.

Wind speed [m/s]	Power [kW]	Thrust coefficient [-]	Power coefficient [-]
4	42.0	0.856	0.201
5	136.0	0.851	0.333
6	276.0	0.838	0.391
7	470.0	0.858	0.420
8	727.0	0.886	0.438
9	1043.0	0.861	0.442
10	1394.0	0.763	0.427
11	1738.0	0.666	0.400
12	2015.0	0.592	0.357
13	2183.0	0.455	0.304
14	2260.0	0.347	0.252
15	2288.0	0.271	0.208
16	2297.0	0.221	0.172
17	2299.0	0.179	0.143
18	2300.0	0.152	0.121
19	2300.0	0.129	0.103
20	2300.0	0.109	0.088
21	2300.0	0.095	0.076
22	2300.0	0.082	0.066
23	2300.0	0.073	0.058
24	2300.0	0.063	0.051
25	2300.0	0.056	0.045

Figure 33: Power curve of the Bonus B82/2300 wind turbine.
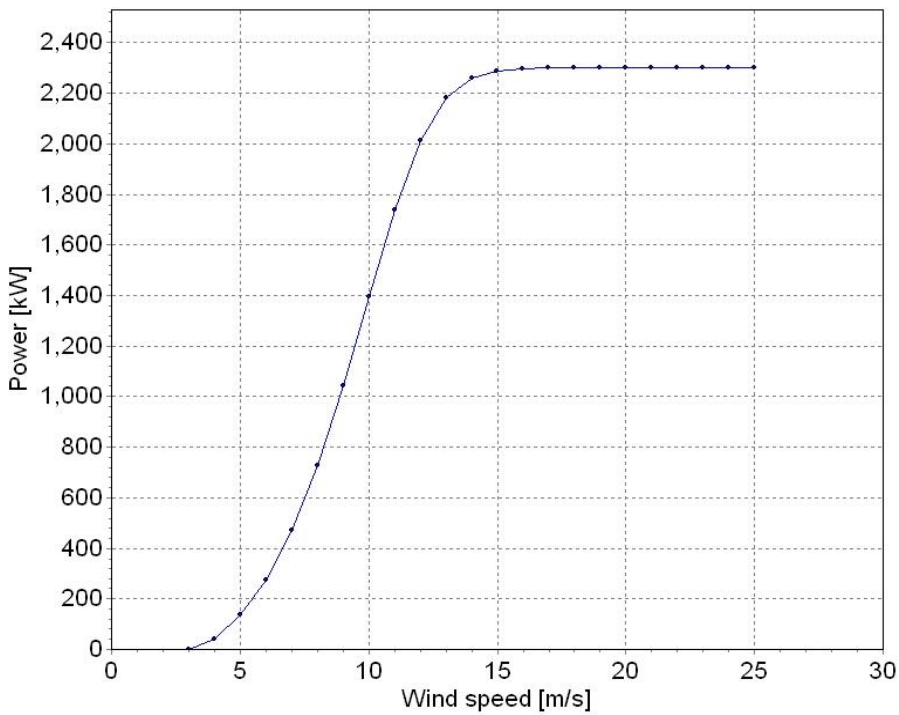
Figure 34: Power and thrust coefficients of the Bonus B82/2300 wind turbine.
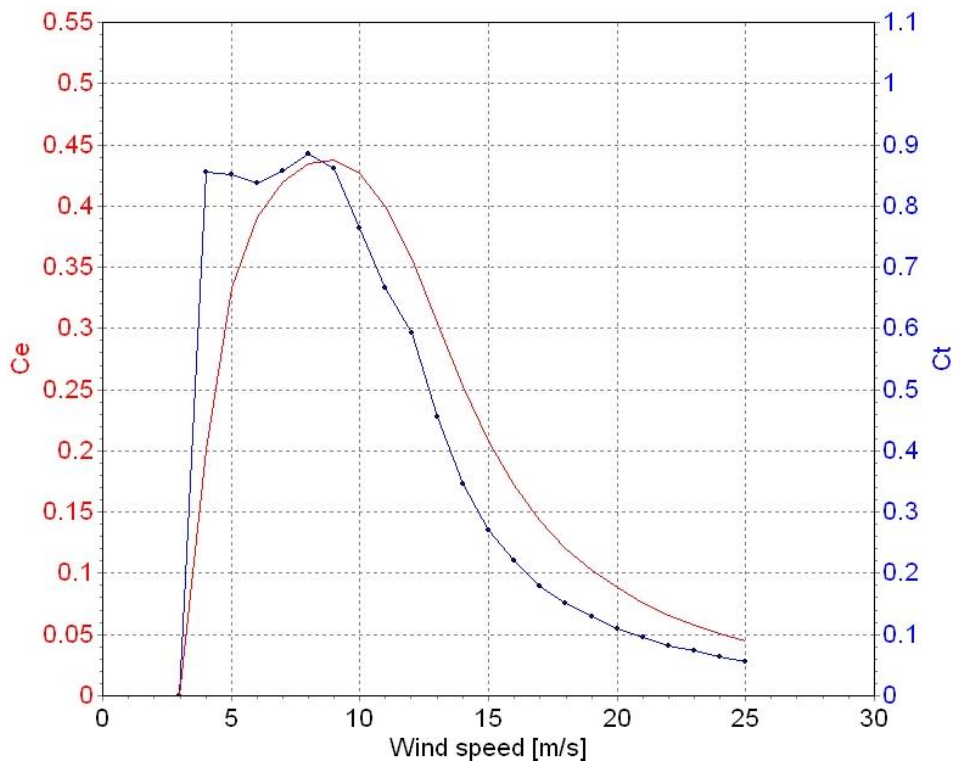
5.3 Ambient conditions

Power recordings of all turbines are available for wind speeds between 6 and 10 m/s while the wind direction has been along the rows. The ambient wind speed, wind direction and turbulence values have been derived from anemometer recordings of a meteorological mast at 69 m height above MSL, approximately 800 m west of turbine 1 (see Figure 32). Table 9 presents the turbulence intensities as function of wind direction and wind.

Table 9: Turbulence values at 69 m height above MSL.

Wind direction [°]	6 m/s [%]	8 m/s [%]	10 m/s [%]
263	5.36	5.59	5.75
268	5.59	5.46	5.34
273	6.23	5.17	5.23
278	5.46	5.14	5.26
283	5.14	4.86	5.46
288	5.26	5.31	5.55
293	5.57	5.57	5.79

5.4 Results

For the Nysted offshore wind farm, all FarmFlow calculations have been post-processed to account for wind direction uncertainty, assuming a standard deviation of the wind direction change for consecutive samples of $\sigma_{\Delta\theta} = 3.0°$.

Power deficits have been determined from measurements for wind speeds between 260.5° and 295.5°. During these measurements the turbines 1 to 8 (west side of the farm) have an undisturbed inflow. Turbine 7 is used as reference turbine for the normalization of the power deficits. Calculations with FarmFlow are performed for all 5°-wide wind directions bins.

Figure 35, Figure 36, and Figure 37 show the normalized power as a function of the turbine position in the rows. The results are averaged for a wide wind sector (260.5-295.5°) at ambient wind speed of 6, 8, and 10 m/s at hub height. Detailed results for narrow wind sectors (± 2.5°) can be found in Appendix A.

The power deficits calculated with FarmFlow agree very well with the measurements. For the ambient wind speeds of 6 m/s FarmFlow underestimates the maximum wake deficit at the most downstream turbines with 9%, while at 8 m/s FarmFlow overestimates the wake deficit with 4%. At an ambient wind speed of 10 m/s the differences are negligible.

Figure 35: Normalized power as a function of column number in the Nysted wind farm in ambient wind speeds of 6.0 ± 0.5 m/s aligned parallel to the rows ± 17.5°.
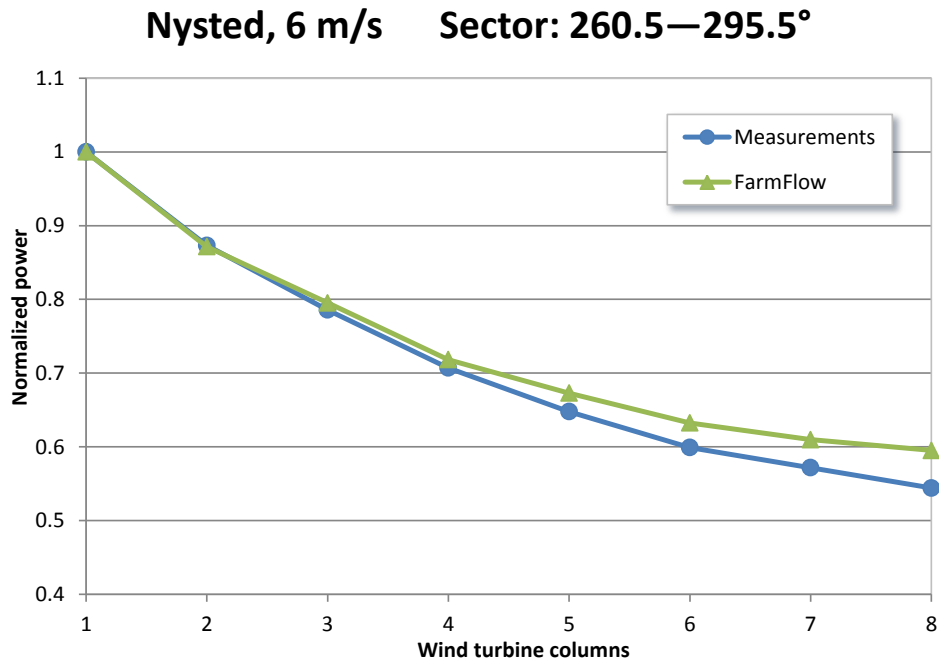
Figure 36: Normalized power as a function of column number in the Nysted wind farm in ambient wind speeds of 8.0 ± 0.5 m/s aligned parallel to the rows ± 17.5°.
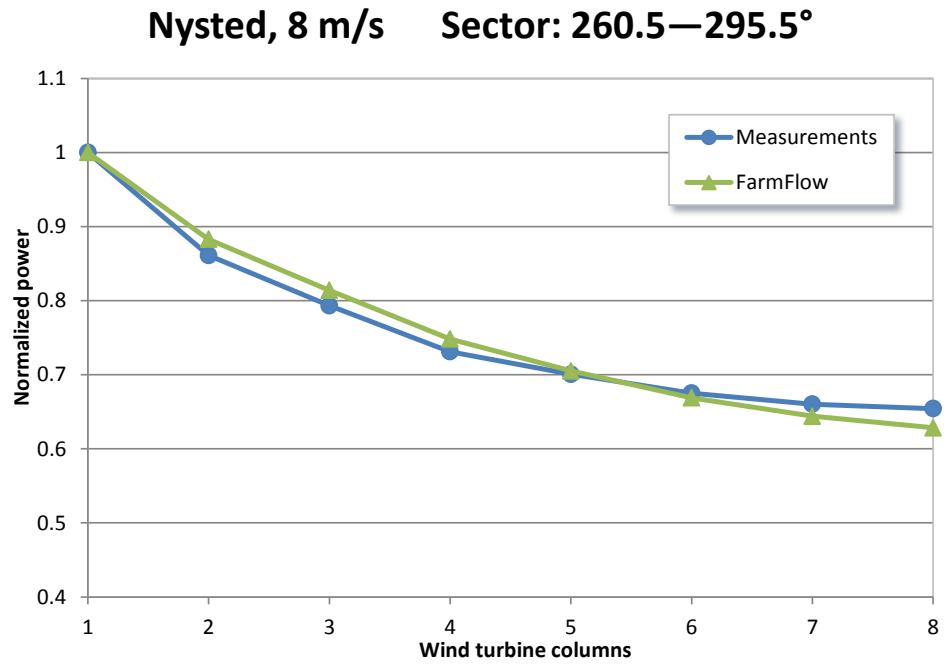
Figure 37: Normalized power as a function of column number in the Nysted wind farm in ambient wind speeds of 10.0 ± 0.5 m/s aligned parallel to the rows ± 17.5°.
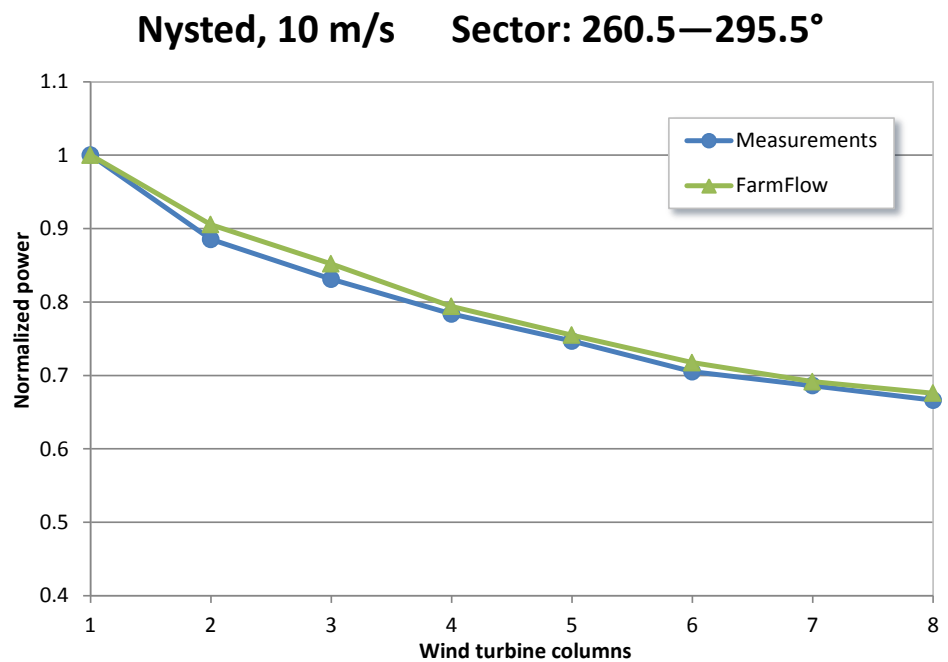
A comparison of the total power deficit of the whole sector for the three wind speeds is given in Table 10. shows the total power deficits for the whole sector. The total power deficit is slightly underestimated with 2.1% at 6 m/s, 0.2% at 8 m/s and 1.1% at 10 m/s.

Table 10: Total power deficit for different wind direction bin sizes.

Wind speed [m/s]	Measured deficit [%]	Calculated deficit [%]	Difference [%]
6	28.4	26.3	-2.1
8	24.1	23.9	-0.2
10	21.2	20.0	-1.1

Figure 38 shows the development of the mean wind speed at hub height through and behind the Nysted wind farm for different widths of the wind direction sector with an average wind direction of 280°. The measurements include wind speeds at distances of 2 and 6 km from the wind farm, where two meteorological masts are installed (see Figure 32). Especially for the wind direction sector width of 3°, 6° and 10°, the FarmFlow results show excellent agreement with all measured data. The calculated wind speed deficits at the meteorological mast downstream Nysted are slightly overestimated by FarmFlow. The wake model of FarmFlow may have a natural tendency of underestimating the recovery of wind turbine wakes at very long distances downstream, due to the fact that no inflow of air (mass) is allowed from outside the computational domain.

Figure 38: Measured (upper) and calculated (lower) wind speed deficit at hub height through and behind the Nysted wind farm for a wind direction of 280° and varying sizes of the wind direction sector.
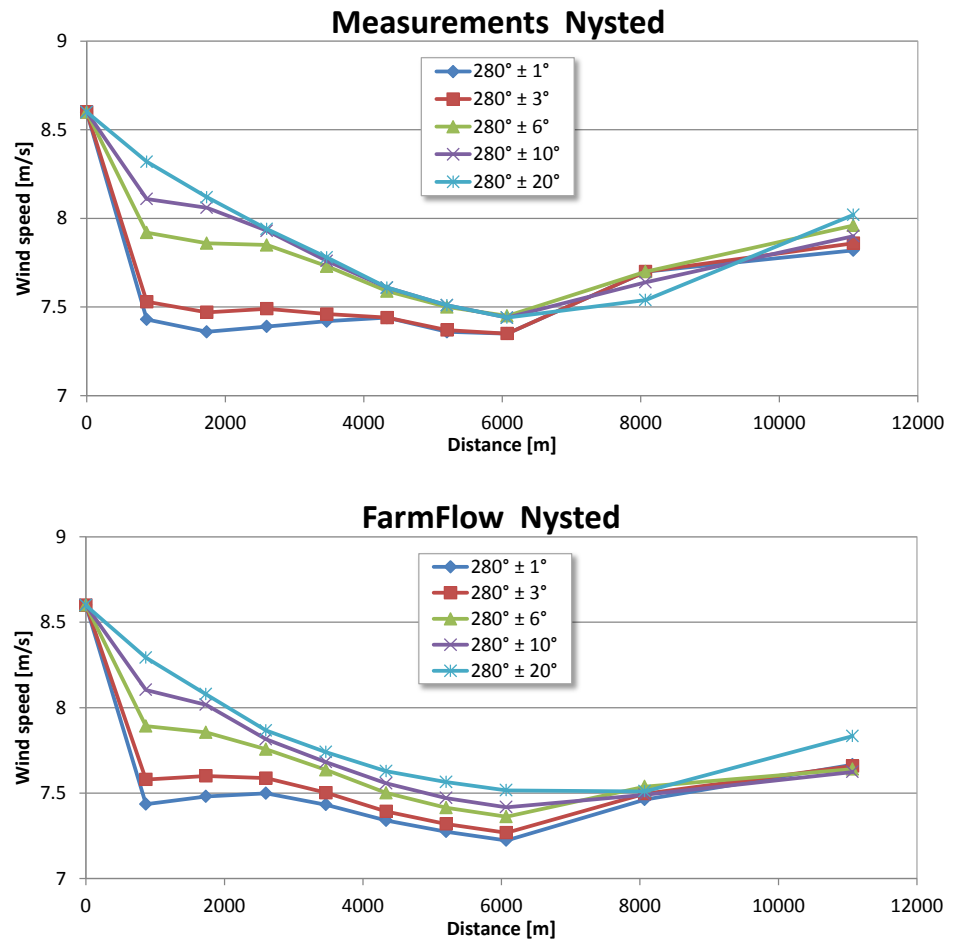
6

OWEZ

6.1   Farm layout

The OWEZ wind farm with a capacity of 108 MW consists of 36 Vestas V90-3.0 MW wind turbines [21]. The pitch controlled wind turbines with rotor diameters of 90 m and hub heights of 70 m above sea level are aligned in 4 rows of 7, 8, 9, and 12 turbines, as indicated in Figure 39.

On the south-west side of the farm a meteorological mast is installed. Wake effects have been measured at hub heights within the wind sectors 0 – 35°, 58 – 76° and 92 – 110°. Within these sectors both single and double wake effects of several wind turbines with distances between 4.3D to 38.9D from the meteorological mast have been measured.

6.2   Turbine data

The turbine data for the Vestas V90-3.0 MW are listed in Table 11. These turbines have rotor diameters of 90 m and hub heights of 70 m above mean sea level (MSL). The official power curve [23] is shown in Figure 41, and the thrust curve and power coefficients are shown in Figure 42. As the Vestas V90-3.0 MW is a pitch controlled variable speed wind turbine, with constant tip speed ratio and pitch angle at low to medium wind speeds, the thrust coefficient is almost constant up to 9 m/s.

Figure 39: Layout of the OWEZ wind farm.
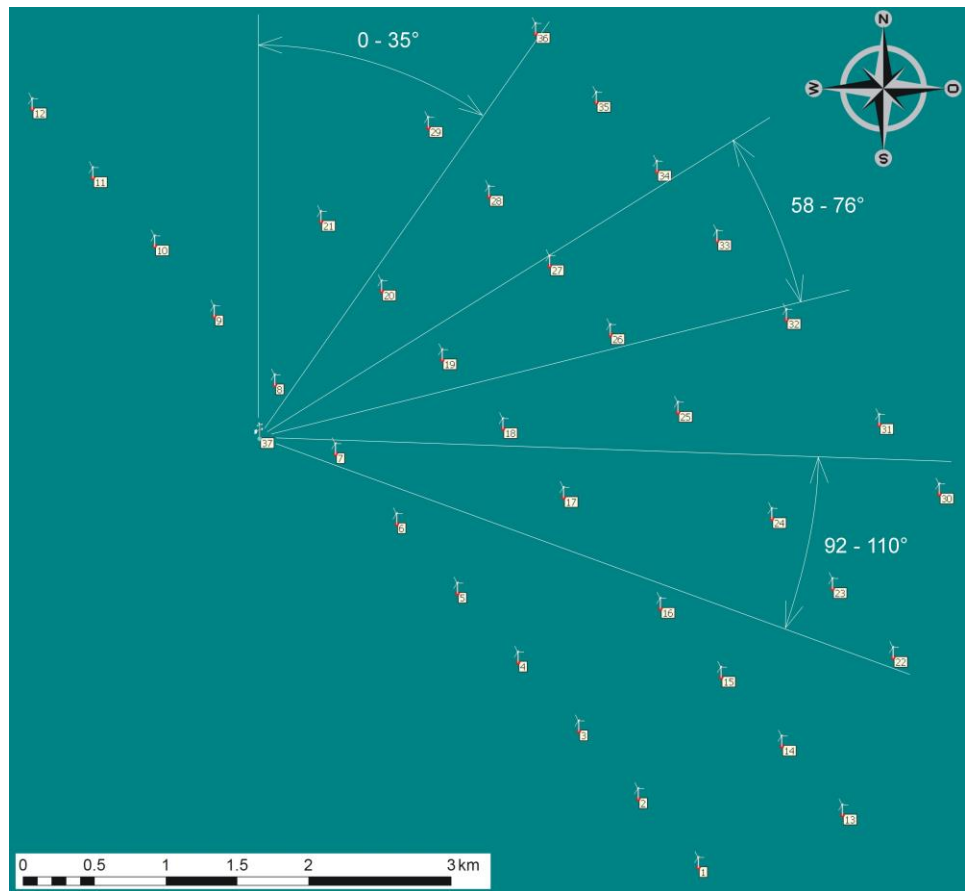
Table 11: Vestas V90-3.0 MW power and thrust data.

Wind speed [m/s]	Power [kW]	Thrust coefficient [-]	Power coefficient [-]
3	0.0	0.845	0.000
4	77.0	0.845	0.309
5	190.0	0.826	0.390
6	353.0	0.825	0.419
7	581.0	0.824	0.435
8	886.0	0.824	0.444
9	1273.0	0.802	0.448
10	1710.0	0.724	0.439
11	2145.0	0.638	0.414
12	2544.0	0.555	0.378
13	2837.0	0.474	0.331
14	2965.0	0.386	0.277
15	2995.0	0.305	0.228
16	3000.0	0.248	0.188
17	3000.0	0.205	0.157
18	3000.0	0.172	0.132
19	3000.0	0.147	0.112
20	3000.0	0.126	0.096
21	3000.0	0.110	0.083
22	3000.0	0.096	0.072
23	3000.0	0.085	0.063
24	3000.0	0.075	0.056
25	3000.0	0.067	0.049

Figure 40: Power curve of the Vestas V90-3.0 MW wind turbine.
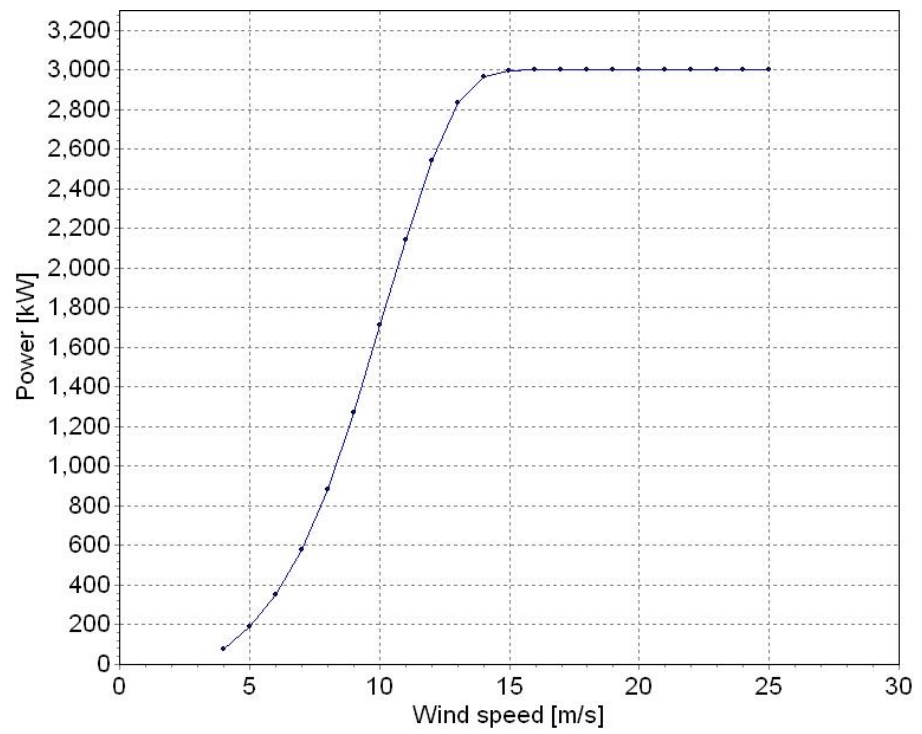
Figure 41: Power and thrust coefficients of the Vestas V90 wind turbine.
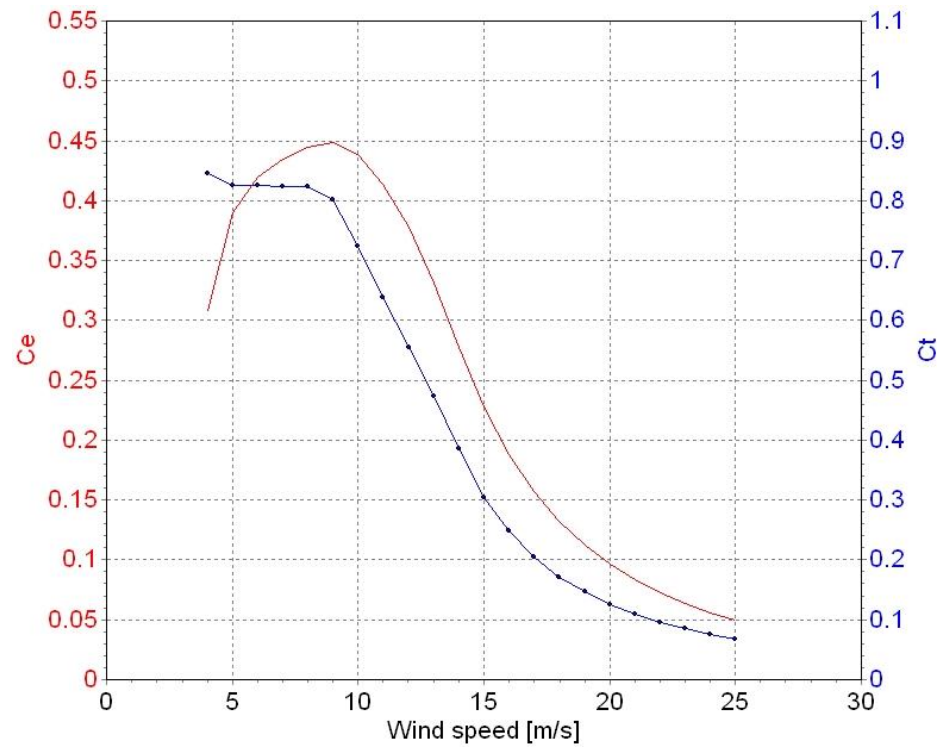
6.3 Ambient conditions

Table 12 shows the annual average wind speed at 70 m above MSL. The data is derived from the meteorological measurements in the period between 01-07-2005 and 31-12-2006 [21]. In the last half year of this period the wind turbines were installed. The wind turbines became active not before 2007.

Figure 42 shows the turbulence intensity as a function of the wind direction. Also these measurements were recorded in the period before the wind farm became active [22] .

Table 12: Annual average wind speed at 70 above MSL.

Sector [°]	Frequency [%]	Weibull A [m/s]	Weibull k	Wind speed [m/s]	Power density [W/m^2]
0	7.54	8.5	2.4	7.54	430
30	5.26	8.4	2.4	7.45	415
60	7.04	8.9	2.7	7.92	458
90	6.68	8.2	2.9	7.31	346
120	4.99	8.0	2.5	7.10	349
150	6.50	9.4	2.7	8.36	539
180	7.43	10.7	2.4	9.49	854
210	12.54	12.3	2.7	10.94	1204
240	12.52	10.9	2.5	9.67	978
270	10.05	9.6	2.4	8.51	618
300	10.36	9.8	2.3	8.68	678
330	9.08	9.2	2.0	8.16	638
All	99.99	9.8	2.5	8.69	677

Figure 42: Turbulence intensity as a function of wind direction as used in the FarmFlow calculations. The measurements (lower figure) are recorded before the wind farm became active.
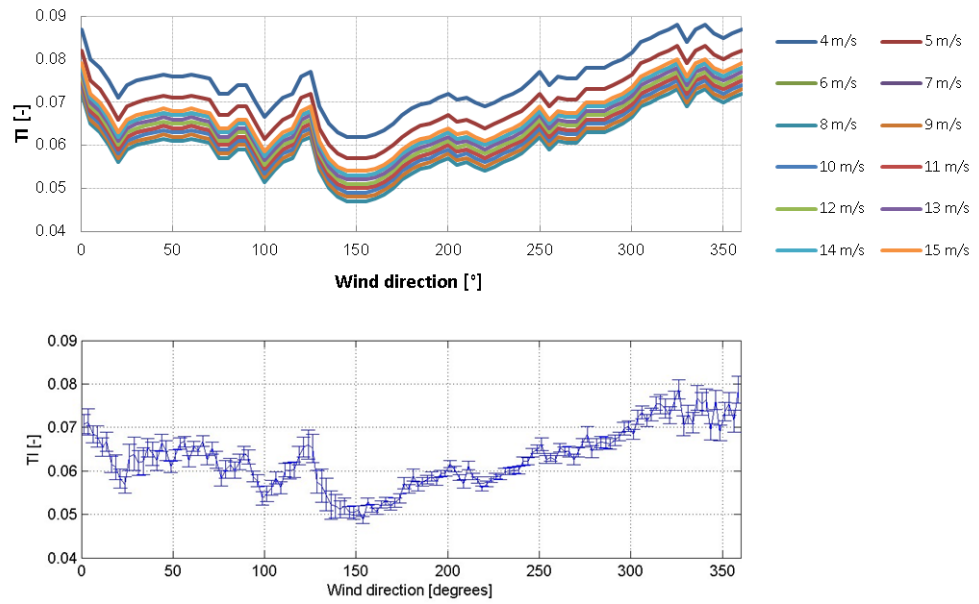
6.4 Results

Wake effects have been measured with the meteorological mast south-west of the wind farm. Measured data has been selected with wind speeds between 4 and 11.5 m/s at hub height, which corresponds to thrust coefficients between 0.6 and 0.82 (see Table 11). The FarmFlow calculations have been performed for ambient wind speeds between 5 and 11.5 m/s at hub height, and corresponding to the 5°-wide wind direction bins. Weibull data of Table 12 has been used to average the calculated wake effects for each wind direction bin.

6.4.1 Turbines 8 and 21

The turbines 8 and 21 are located north from the meteorological mast (at 16°), at a distance of 4.3D and 17.6D respectively (see Figure 39). Figure 43 shows the measured and calculated turbulence intensities for all configurations of operating and non-operating turbines. The calculated results from FarmFlow show approximately the same levels of turbulence as the measurements. However, the measurements show maximum turbulence levels near the edge of the wake, while the FarmFlow calculations show maximum values in the centre of the wakes.

The meteorological mast detects wake effects from turbine 29 for wind directions >25°. Unfortunately, it is unknown if this turbines was operating all the time during these measurements.

Figure 43: Measured (left) and calculated (right) turbulence intensities at hub height as a function of the wind direction. The graphs show Weibull averaged turbulence intensities of all combinations of operating (on) and not operating (off) turbines for ambient wind speeds between 5 and 11.5 m/s.
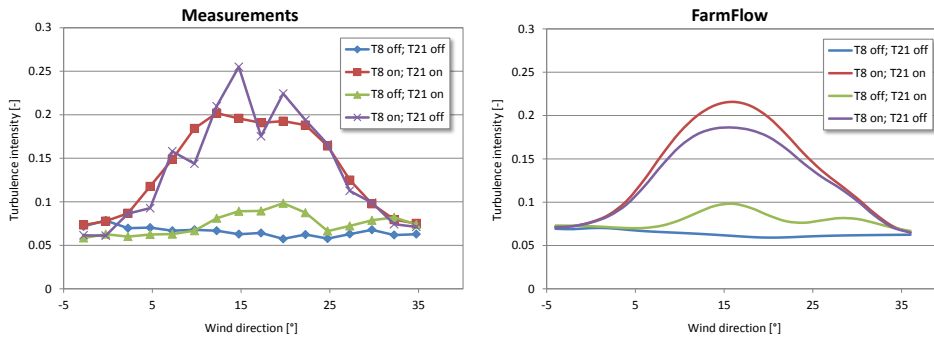
A comparison of measured and calculated turbulence intensities from a single wake for a rotor distance of 4.3*D* is shown in Figure 44. The turbulence intensity in the centre of the wake at this relatively short distance is approximately 0.2. The FarmFlow results agree reasonably well with the measurements. At a much larger distance of 17.6*D*, the maximum turbulence intensity is reduced to approximately 0.1. (see Figure 45). Apart from a small offset of approximately 4° in the wind direction, the FarmFlow results agree quite well with the measurements.

Figure 46 shows a comparison of the measured and calculated turbulence intensity from double wakes of turbines 8 and 21. Again, the graph shows a very good agreement between the measured and calculated results.

Figure 44: Measured and calculated single wake turbulence at a rotor distance of 4.3*D* at hub height as a function of the wind direction.
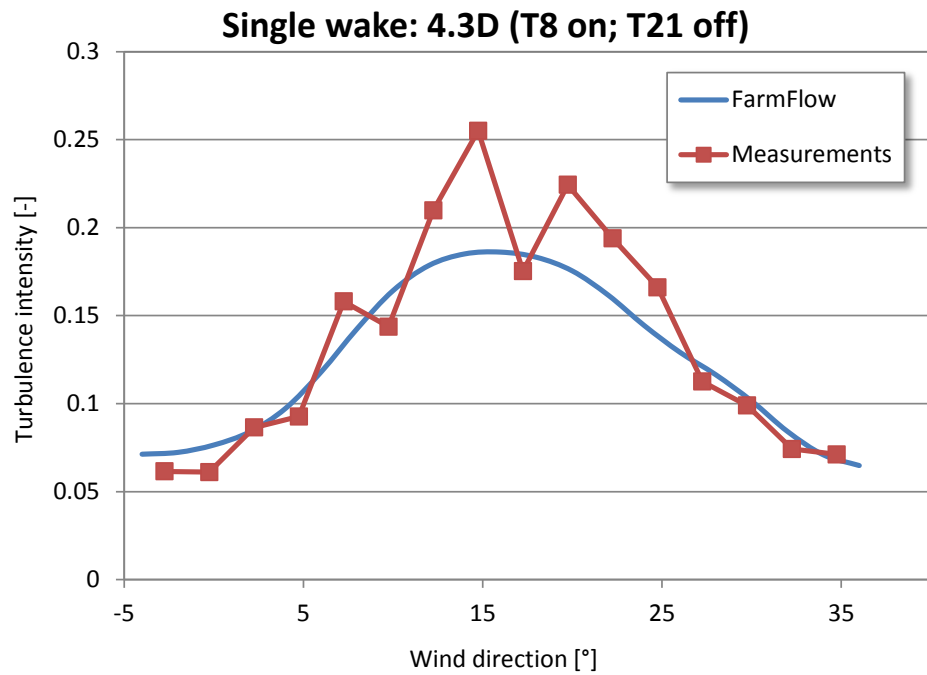
Figure 45: Measured and calculated single wake turbulence at a rotor distance of 17.6*D* at hub height as a function of the wind direction.
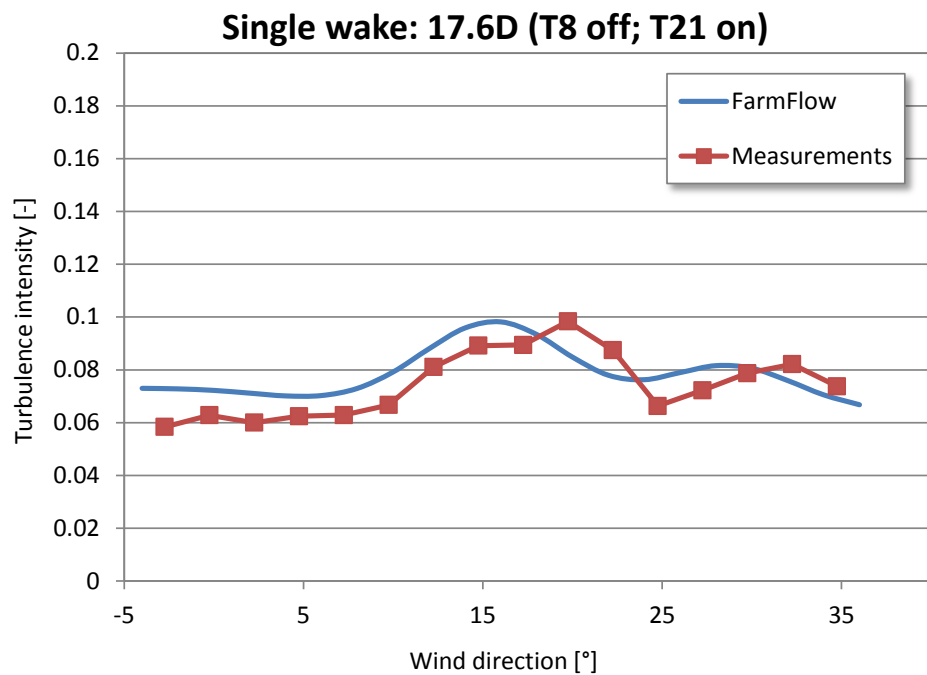
Figure 46: Measured and calculated double wake turbulence at a rotor distance of 4.3*D* and 17.6*D* at hub height as a function of the wind direction.
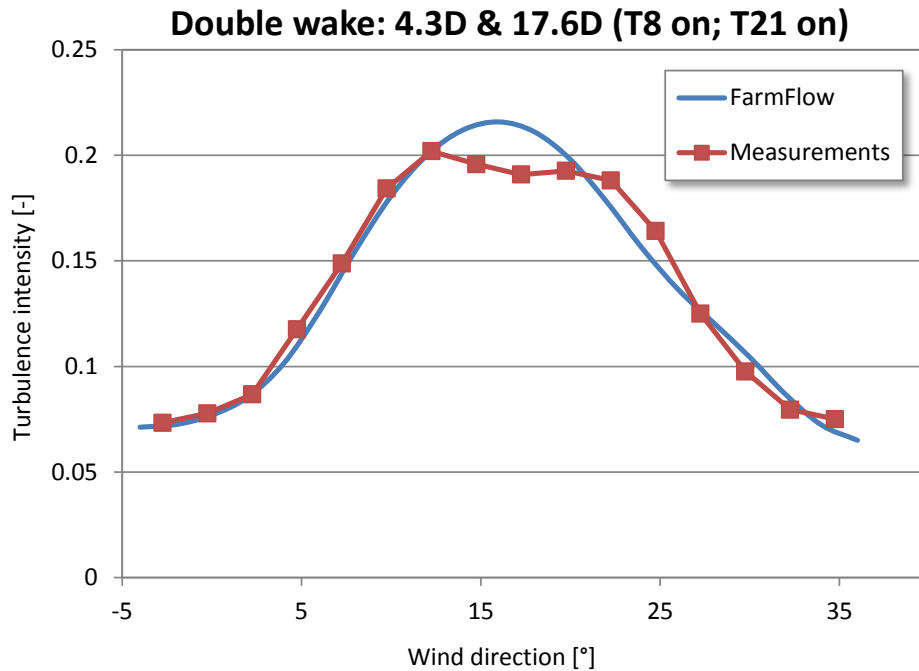
6.4.2 Turbines 19 and 33

The turbines 19 and 33 are located north-east from the meteorological mast (67°), at very large distances of 15.5*D* and 38.9*D* respectively (see Figure 39). Figure 47 shows the measured and calculated turbulence intensities for all configurations of operating and non-operating turbines. According to the measurements, the added turbulence is only 0.025 at a distance of 15.5*D*. The added turbulence intensity at 38.9*D* is less than 0.01. In the centre of the wake, the added turbulence intensity calculated by FarmFlow is overestimated slightly. On the other hand, it is rather unexpected that the measured turbulence intensity in the wake of turbine 19 (purple crosses of Figure 47) is lower than the measured turbulence intensity in the wake of turbine 21 (green triangles of Figure 43), which is located closer to the meteorological mast. Regarding this distance, the results of FarmFlow are more consistent than the measured turbulence intensities.

At 60° and 75° the FarmFlow results show clearly the wake effects of turbines 27 and 26 respectively. It is not clear if these turbines were (always) operating during the measurements.

Figure 47: Measured (left) and calculated (right) turbulence intensities at hub height as a function of wind direction. The graphs show Weibull averaged turbulence intensities of all combinations of operating (on) and not operating (off) turbines for ambient wind speeds between 5 and 11.5 m/s.
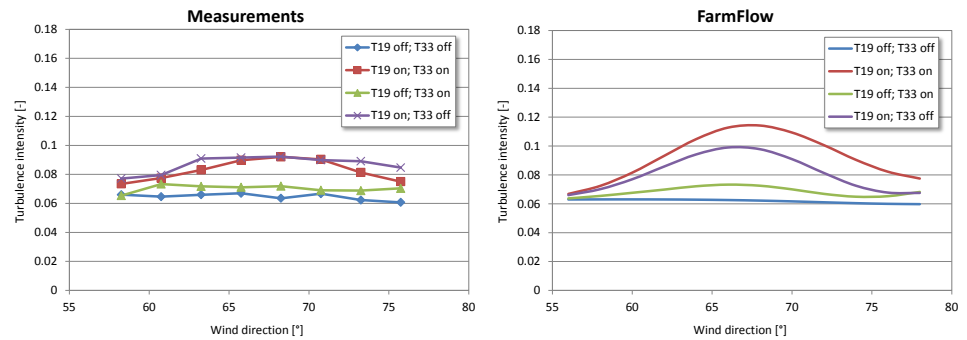
A comparison of measured and calculated turbulence intensity from a single wake for a rotor distance of 15.5*D* and 38.8*D* is shown in Figure 48 and Figure 49 respectively. A comparison of the double wake effect from both turbines is shown in Figure 50.

Figure 48: Measured and calculated single wake turbulence at a rotor distance of 15.5*D* at hub height as a function of wind direction.
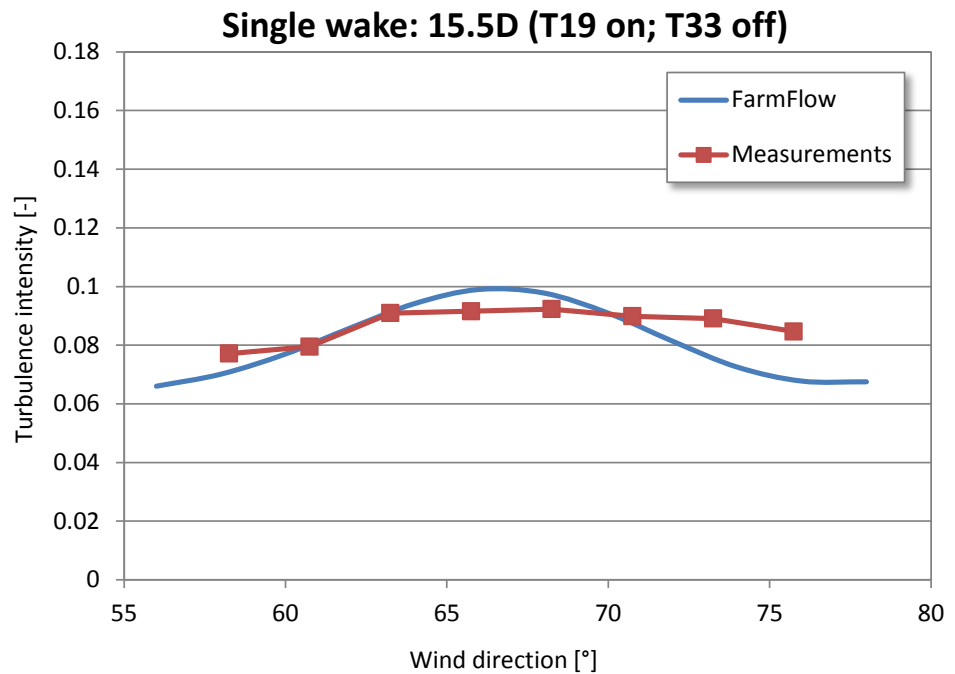
Figure 49: Measured and calculated single wake turbulence at a rotor distance of 38.9*D* at hub height as a function of wind direction.
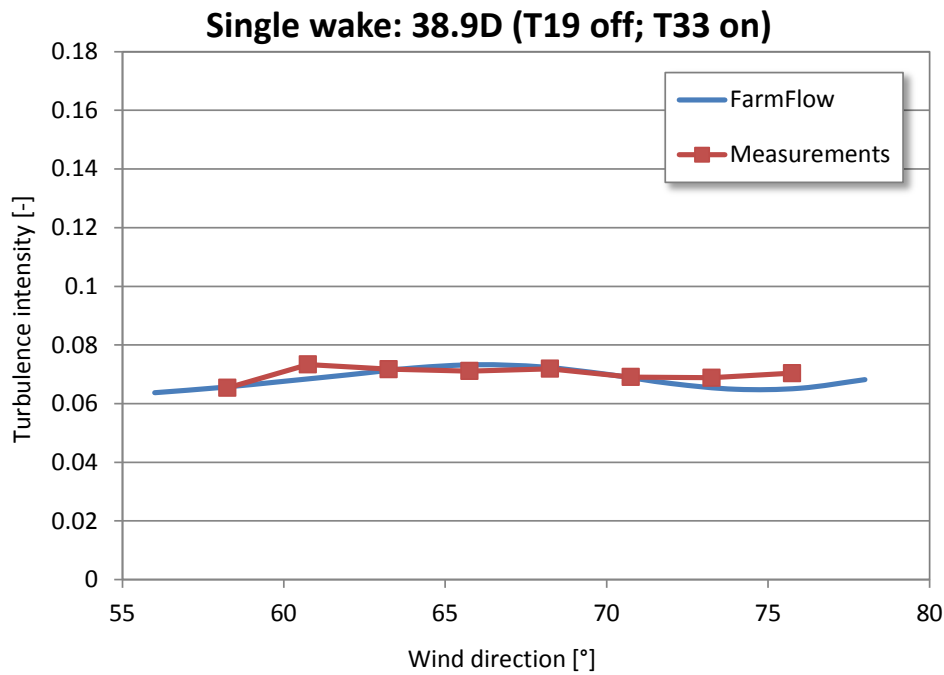
Figure 50: Measured and calculated double wake turbulence at a rotor distance of 15.5*D* and 38.9*D* at hub height as a function of wind direction.
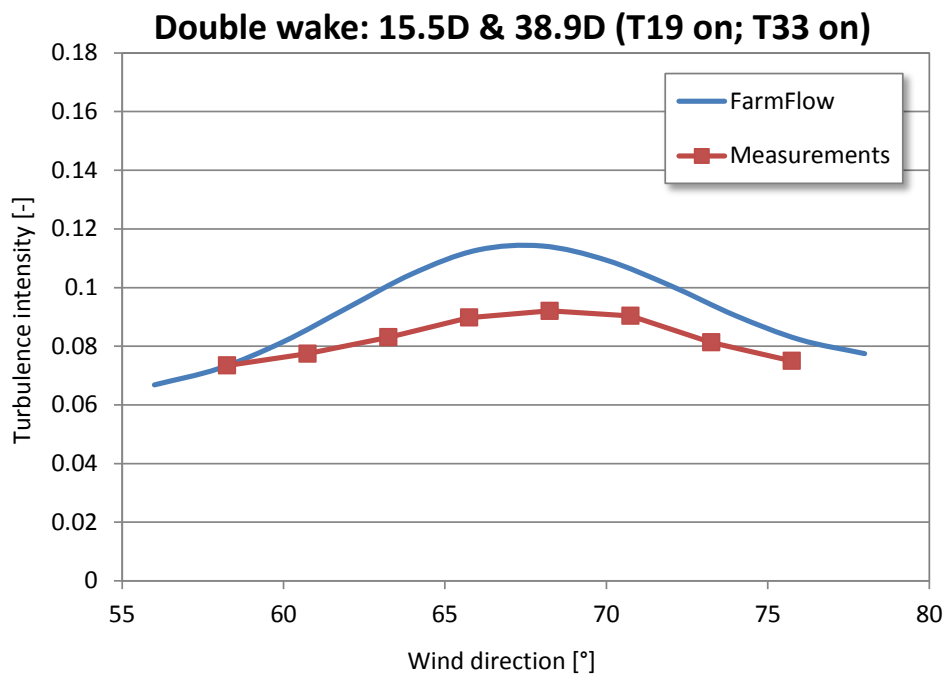
6.4.3 Turbines 7 and 17

The turbines 7 and 17 are located east from the meteorological mast (101°), at a distance of 6.0D and 24.1D respectively (see Figure 39). Figure 51 shows the measured and calculated turbulence intensities for all configurations of operating and non-operating turbines. According to the measurements, the maximum turbulence intensity in the centre of the wake is approximately 0.15 at a distance of 6.0D, and 0.09 at 24.1D. The maximum turbulence intensity in the centre of the wake calculated by FarmFlow overestimated with approximately 0.03.

Figure 51: Measured (left) and calculated (right) turbulence intensities at hub height as a function of wind direction. The graphs show Weibull averaged turbulence intensities of all combinations of operating (on) and not operating (off) turbines for ambient wind speeds between 5 and 11.5 m/s.
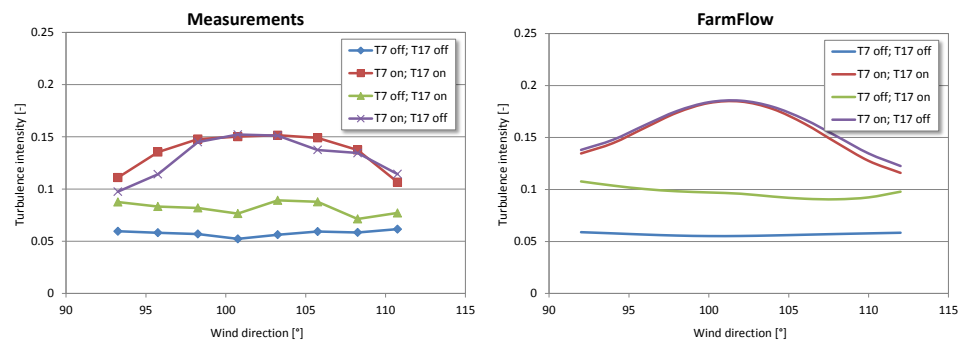
A comparison of measured and calculated turbulence intensities from a single wake for a rotor distance of 15.5D and 38.8D is shown in Figure 52 and Figure 53 respectively. A comparison of double wake effects from both turbines is shown in Figure 54.

Figure 52: Measured and calculated single wake turbulence at a rotor distance of 6.0D at hub height as a function of wind direction.
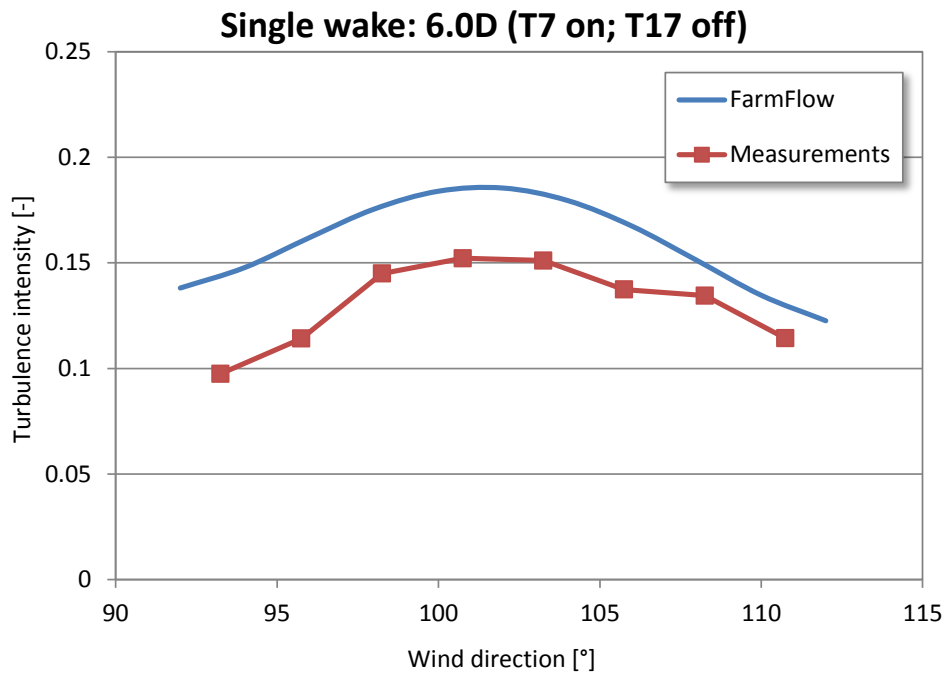
Figure 53: Measured and calculated single wake turbulence at a rotor distance of 24.1D at hub height as a function of wind direction.
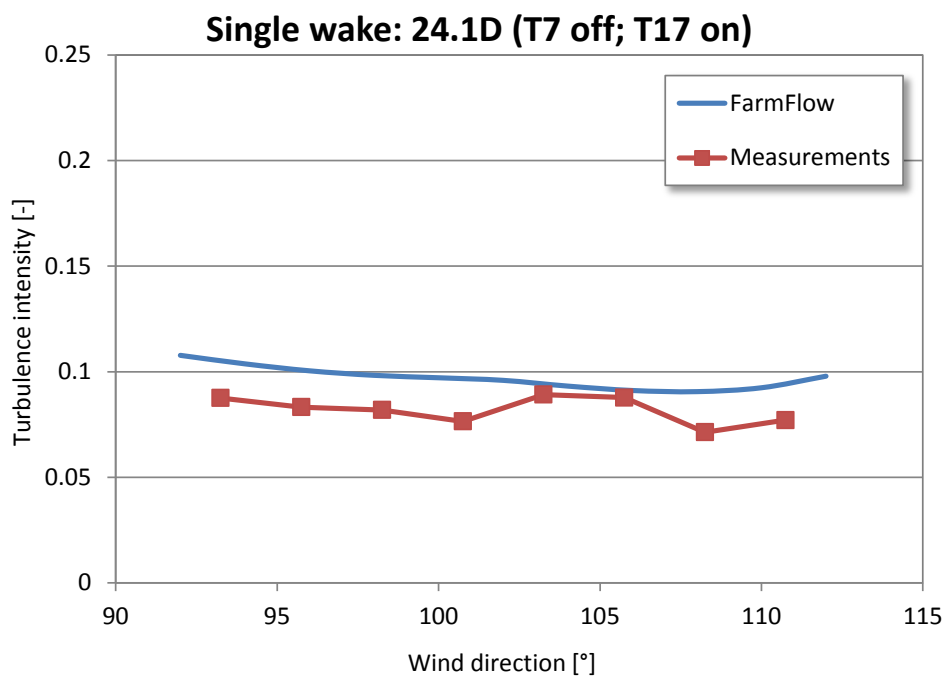
Figure 54: Measured and calculated double wake turbulence at a rotor distance of 6.0D and 24.1D at hub height as a function of wind direction.
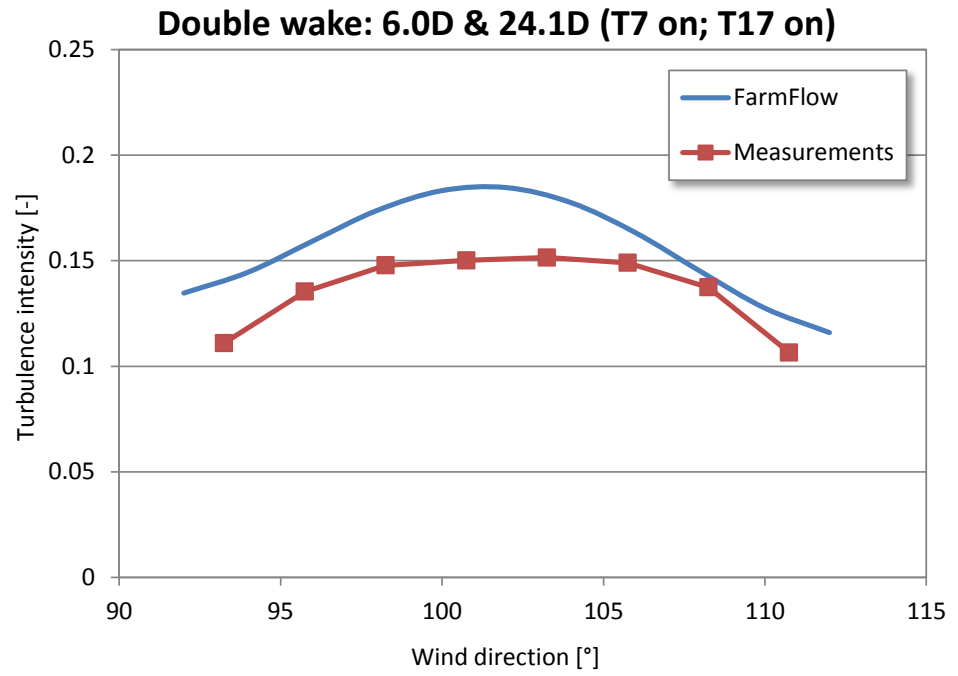
7
Conclusions

With the development of the wind turbine wake modelling tool FarmFlow, ECN is able to calculate the power production of large offshore wind farms with the highest accuracy possible today. Various blind benchmark studies between 2009 and 2014 proved that FarmFlow provides the highest accuracy for large offshore wind farms in comparison with other wake models [13, 14].

In the period 2012-2014 several modifications and improvements of FarmFlow have been applied. Active Wake Control has been implemented, the computational time has decreased with a factor 20, the development of a batch version for operation on a cluster has been realized, and the boundary layer model has been extended to non-neutral conditions and extreme low turbulence levels.

In this report three large offshore wind farms and the ECN Wind Turbine Test farm (EWTW) have been modelled in FarmFlow. The calculated wake effects have been compared with experimental data from these wind farms.

The calculated wake velocity deficits agree very well with the experimental data when the turbine spacing is 5 rotor diameters or more. Only when an extremely small turbine spacing is applied (i.e. less than 5 rotor diameters) FarmFlow overestimates the wake recovery. For offshore wind farms, the turbine spacing is commonly between 6 and 10 rotor diameters. The comparison with experimental data from the offshore wind farms Horns Rev and Nysted with a turbine spacing of 7 and 10 rotor diameters respectively have shown that wake losses of individual wind turbines are predicted very accurately.

References

[1]   Crespo A. and J. Hernández, *Numerical modelling of the flow field in a wind turbine wake*, Proceedings of the 3rd Joint ASCE/ASME Mechanics Conference, pages 121-127, ASME, 1989.

[2]   Panofsky H.A. and J.A. Dutton, *Atmospheric Turbulence*, Wiley, 1984.

[3]   Crespo A., J. Hernández and S. Frandsen, *Survey of modelling methods for wind turbine wakes and wind farms*, Wind Energy, 1999, Vol. 2, pages 1-24.

[4]   Schepers, J.G., *ENDOW: Validation and improvement of ECN's wake model*, ECN-C--03-034, ECN, 2003.

[5]   Henneman, B., *Numerical aspects of the WAKEFARM program*, ECN-C--03-035, ECN, 2003.

[6]   Dahlberg, J.A., and D. Medici, *Potential improvement of wind turbine array efficiency by active wake control (AWC)*, EWEC 2003, Madrid.

[7]   Van der Pijl, S.P. and J.G. Schepers, *Improvements of the WAKEFARM wake model*, Presented at the Annex XXIII: Offshore wind energy technology and deployment, Workshop on wake modelling and benchmarking of models, 2006.

[8]   Schepers, J.G. and S.P. van der Pijl, *Improved modelling of wake aerodynamics and assessment of new farm control strategies*, Journal of Physics, Conference Series 75, 2007.

[9]   Eecen, P.J. and J.P. Verhoef, *EWTW Meteorological database; Description June 2003 – May 2006*, ECN-E--06-004, 2006.

[10] Machielse, L.A.H., *Validatiemetingen EWTW, Eindrapport*, ECN-E--06-062, 2006.

[11] Machielse, L.A.H. et al., *ECN test farm measurements for validation of wake models*, ECN-M--07-044, EWEC 2007.

[12] Machielse, L.A.H., *Measured wind and performance characteristics in the wake of 2.5MW turbines*, ECN-X--06-130, Confidential, 2007.

[13] Barthelmie, R.J. et al., *Flow and wakes in large wind farms: Final report for UpWind WP8*, Risø-R-1765(EN), 2011.

[14] Hasager, C.B. and G. Giebel, *EERA DTOC final summary report*, D7.20, June 2015.

[15] Hansen, K.S., R.J. Barthelmie, L.E. Jensen, and A. Sommer, *The impact of turbulence intensity and atmospheric stability on power deficits due to wind turbine wakes at Horns Rev wind farm*, Wind Energy, 2012, Vol. 15, pages 183-196.

[16] Jensen, L.E., *Wake measurements from the Horns Rev wind farm*, EWEC 2004, London.

[17] Data file *nystedcoordinates32.csv*, September 2008.

[18] Data file *Bonus 2_3 MW.txt*, September 2008.

[19] Data file *PV_and_CDaxV.xls*, September 2008.

[20] *Hovedspecifikation NM52/900 50 HZ*, TIC027'007 DK, 2001.

[21] Eecen, P.J., L.A.H. Machielse and A.P.W.M. Curvers, *Meteorological measurements OWEZ; Half year report 01-07-2006 – 31-12-2006*, ECN-E--07-075, 2007.

[22] Eecen, P.J., J.W. Wagenaar and E.T.G. Bot, *Offshore wind farms: losses and turbulence in wakes; modelling and validation*, Wake Workshop June 2011, Sweden.

[23] *General Specification V90 – 3.0 MW VCRS*, Item no. 950010.R5, Vestas Wind Systems A/S, 2006-10-18, Denmark.

[24] Kasmi, A. E. and C. Masson, *An extended k–ε model for turbulent flow through horizontal-axis wind turbines*, Journal of Wind Engineering and Industrial Aerodyamics 96 (2008), pages 103-122.

[25] Massouh, F. and I. Dobrev, *Exploration of the vortex wake behind of wind turbine rotor*, J Phys Conf Ser 7 012036 IOP Publishing, 2007.

[26] Dahlberg, J.A., and B. Montgomerie, *Wake effects and other loads* (Final report: part II), Research program of the Utgrunden demonstration offshore wind farm, February 2005.

[27] Schepers, J.G., *Engineering models in wind energy aerodynamics*, Delft, November 2012.

Appendix A. Nysted normalized performance

This appendix shows normalized turbine powers of the wind turbines of the Nysted wind farm as a function of the column number. Measurements are compared with FarmFlow results. The measurements are divided in narrow wind direction bins of 5° wide and wind speed bins of 2 m/s wide with averages of 6, 8, and 10 m/s at hub height. The FarmFlow results are calculated for average wind directions and wind speeds for each bin, and post-processed to account for wind direction uncertainty. A Gaussian distribution with a standard deviation of 3° is assumed for the wind direction change over consecutive 10 minute samples.

Nysted, 6 m/s   Sector: 263±2.5°
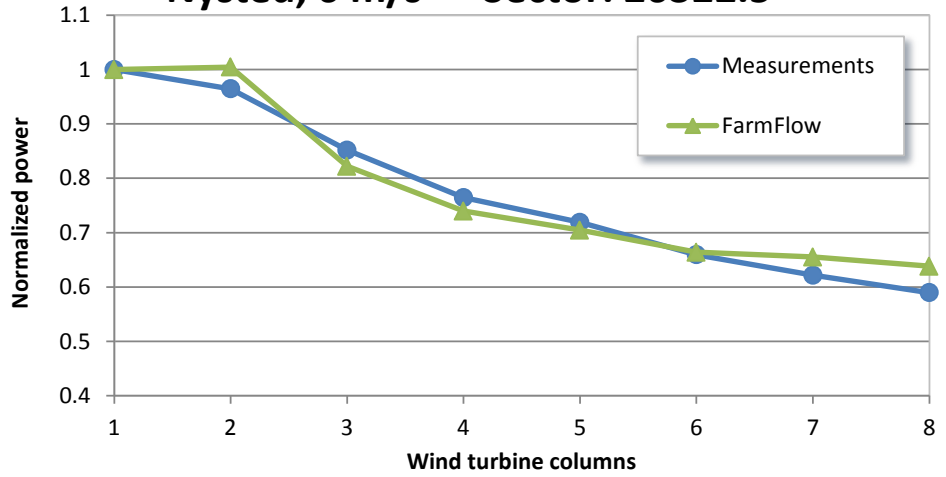
Nysted, 8 m/s   Sector: 263±2.5°
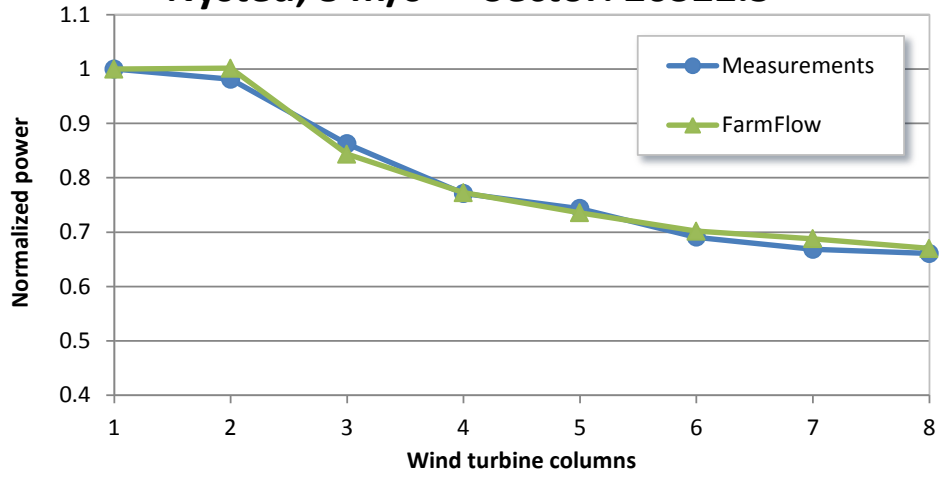
Nysted, 10 m/s   Sector: 263±2.5°

Nysted, 6 m/s   Sector: 268±2.5°

Nysted, 8 m/s   Sector: 268±2.5°

Nysted, 10 m/s   Sector: 268±2.5°
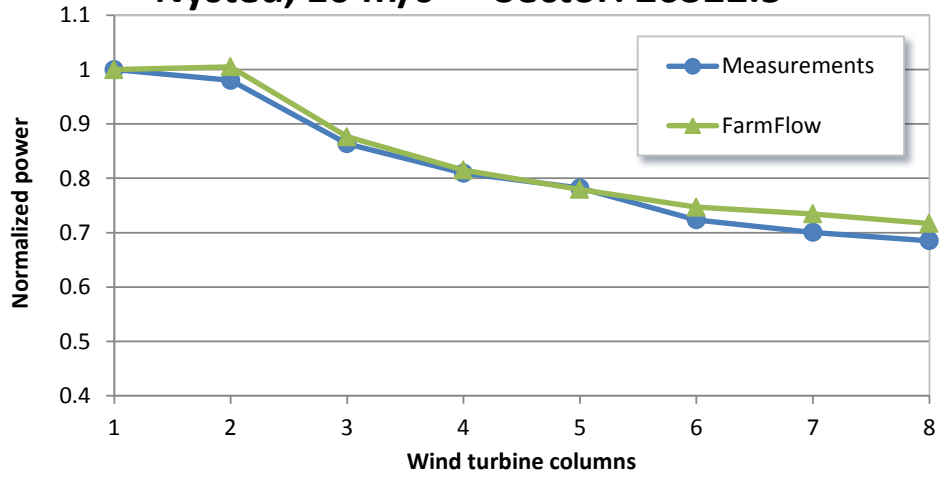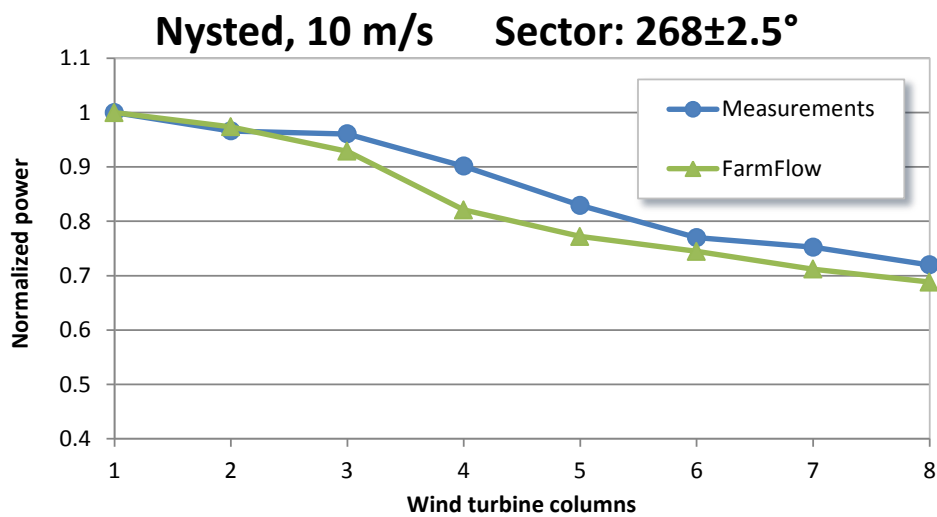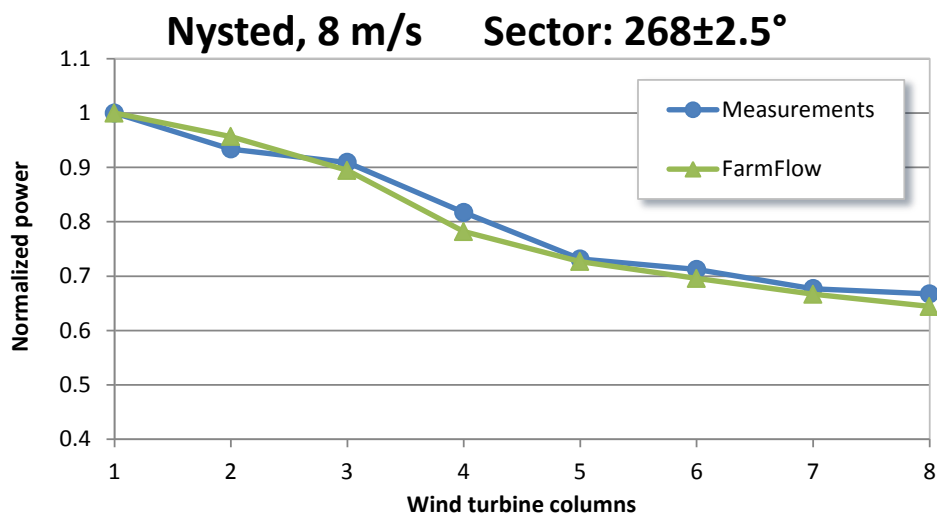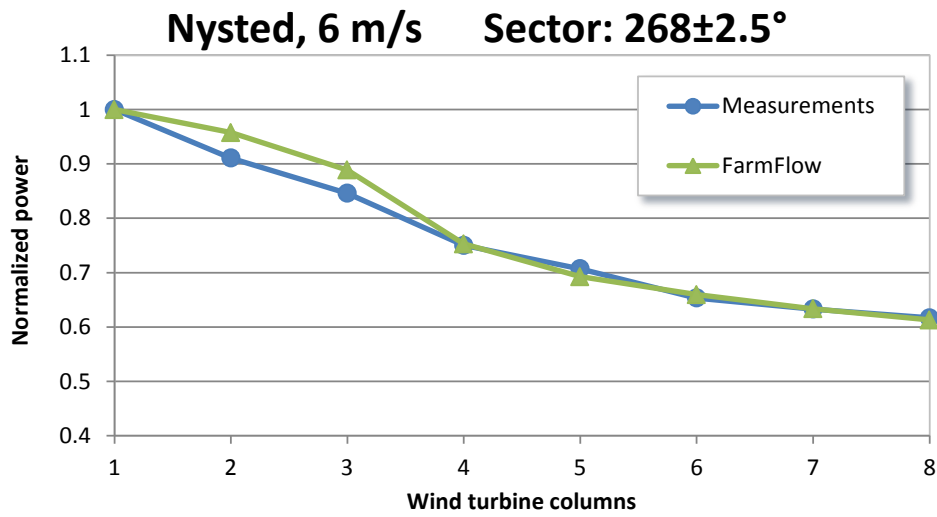
Nysted, 6 m/s   Sector: 273±2.5°
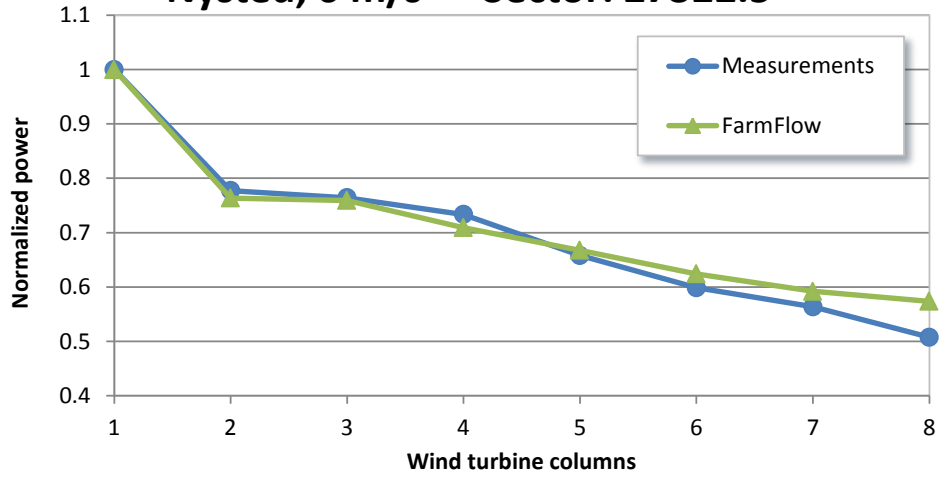
Nysted, 8 m/s   Sector: 273±2.5°
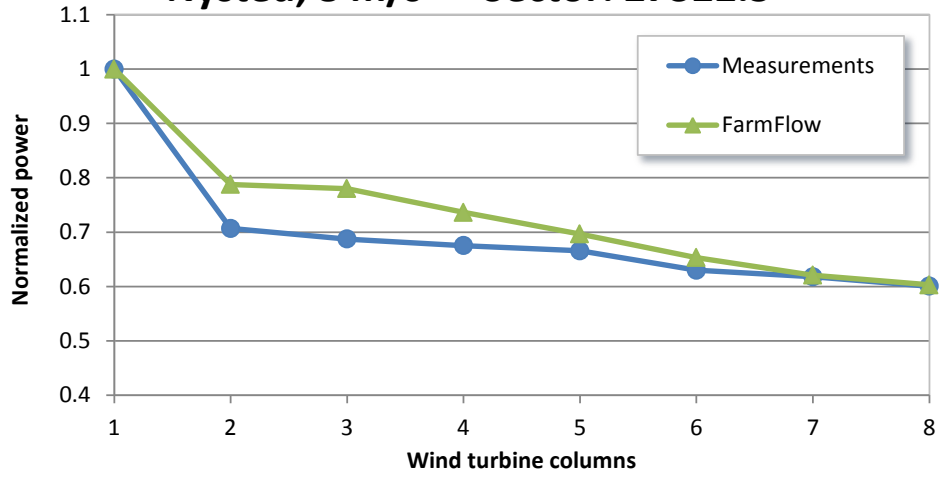
Nysted, 10 m/s   Sector: 273±2.5°

Nysted, 6 m/s   Sector: 278±2.5°

Nysted, 8 m/s   Sector: 278±2.5°

Nysted, 10 m/s   Sector: 278±2.5°
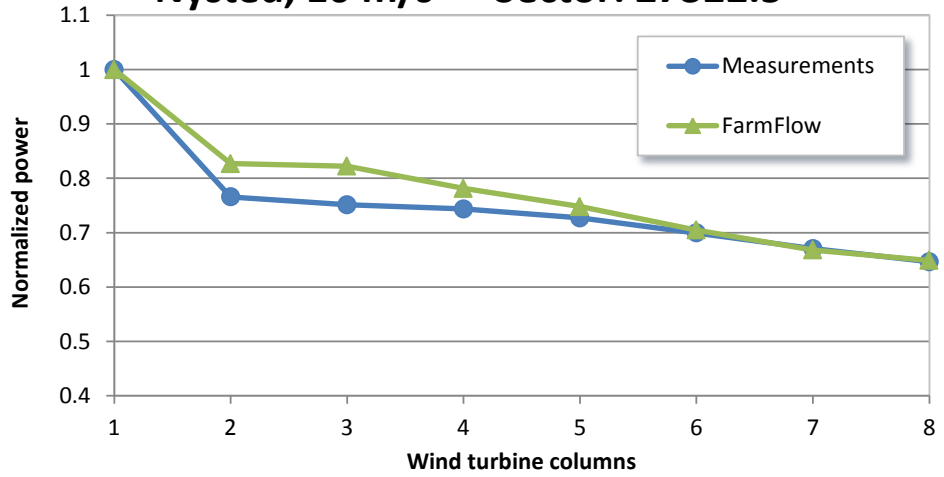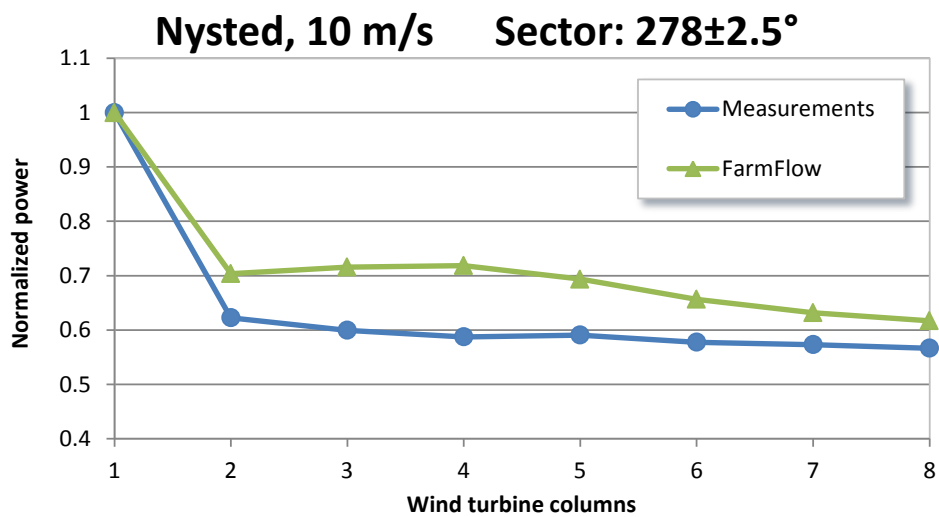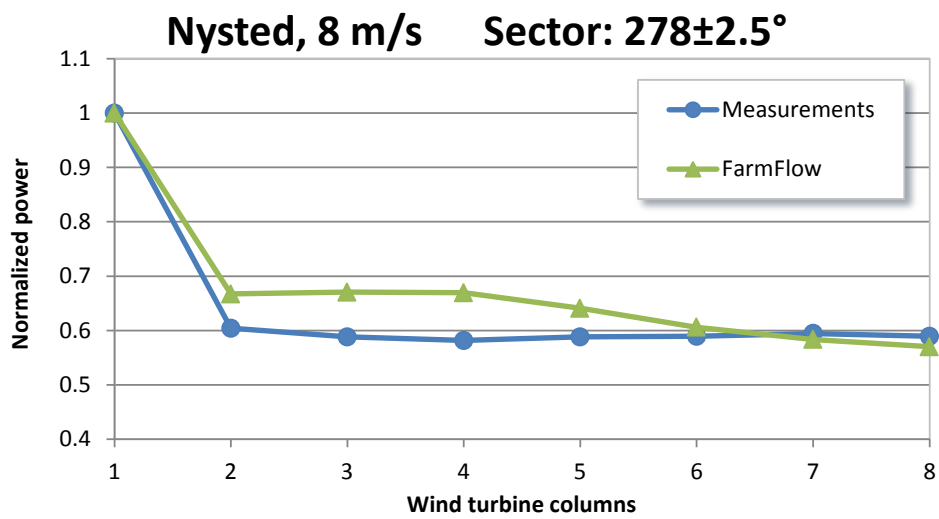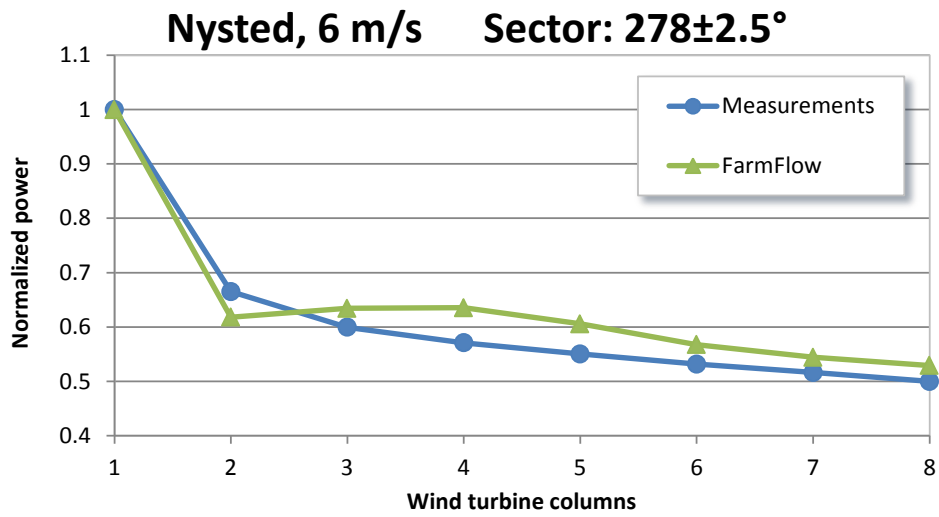
Nysted, 6 m/s   Sector: 283±2.5°
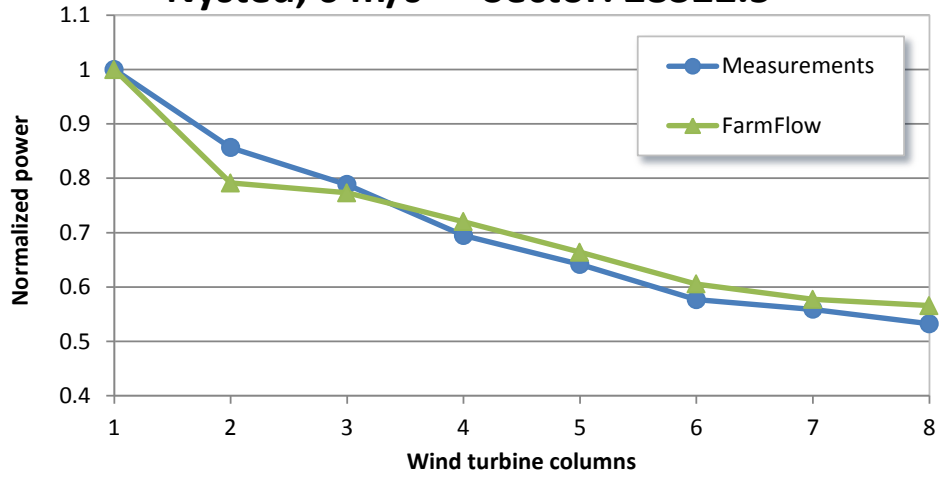
Nysted, 8 m/s   Sector: 283±2.5°
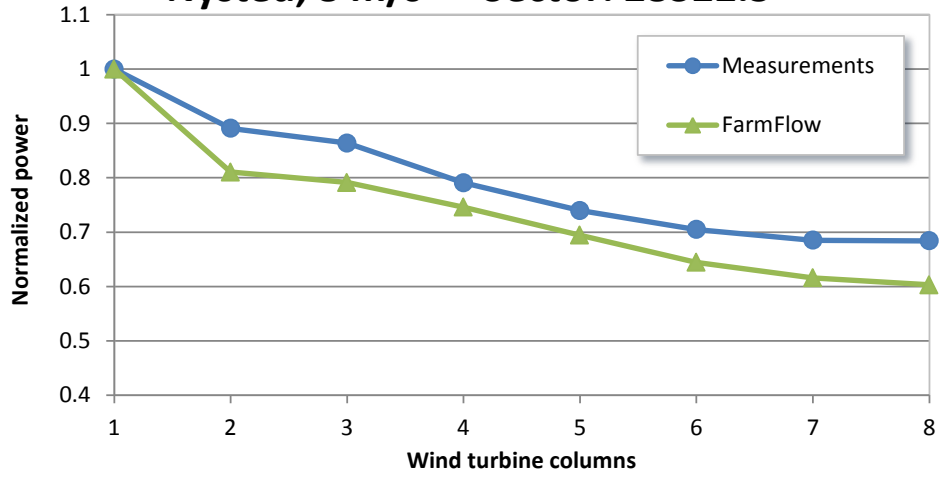
Nysted, 10 m/s   Sector: 283±2.5°

Nysted, 6 m/s   Sector: 288±2.5°

Nysted, 8 m/s   Sector: 288±2.5°

Nysted, 10 m/s   Sector: 288±2.5°
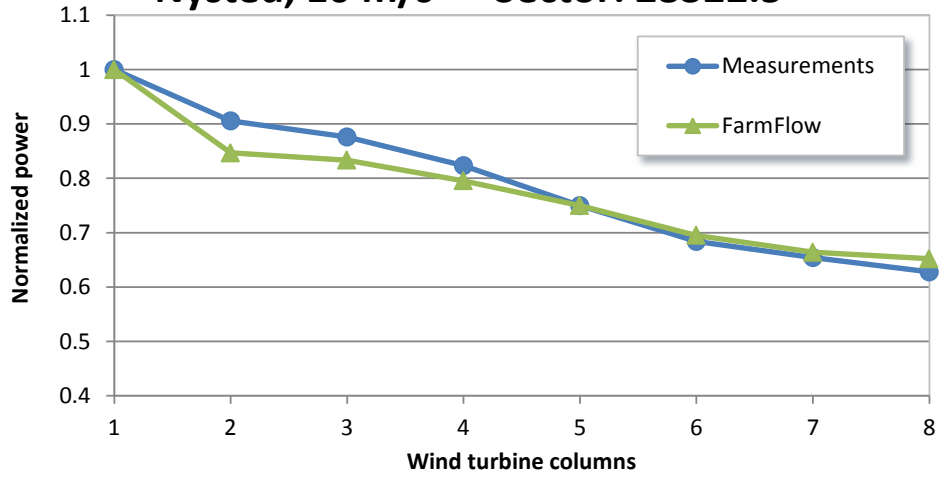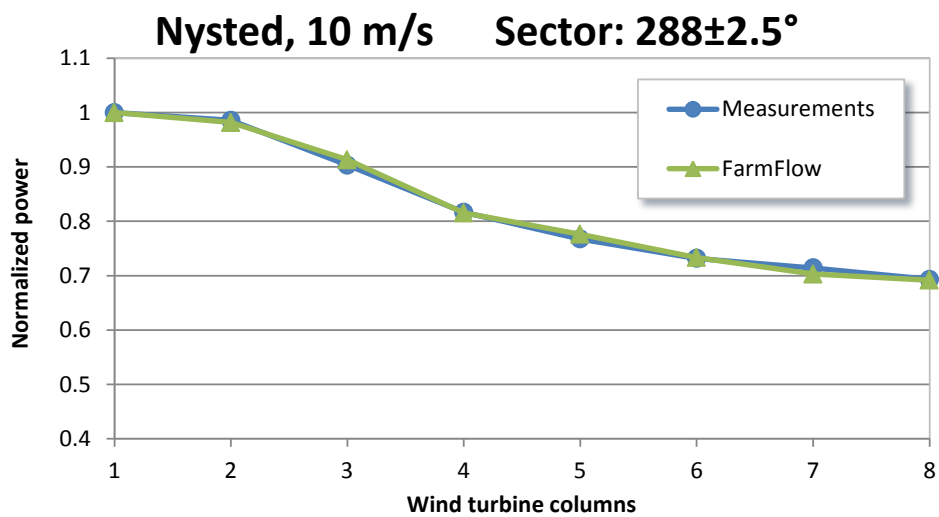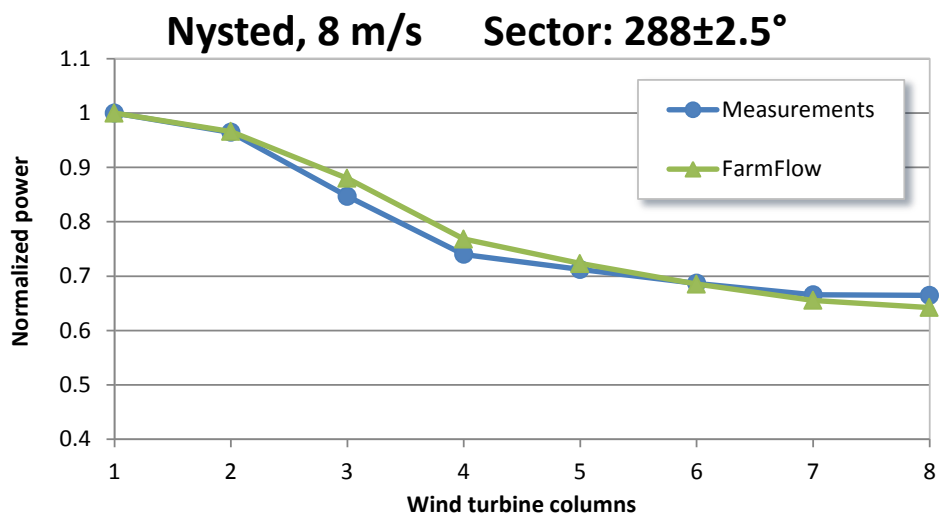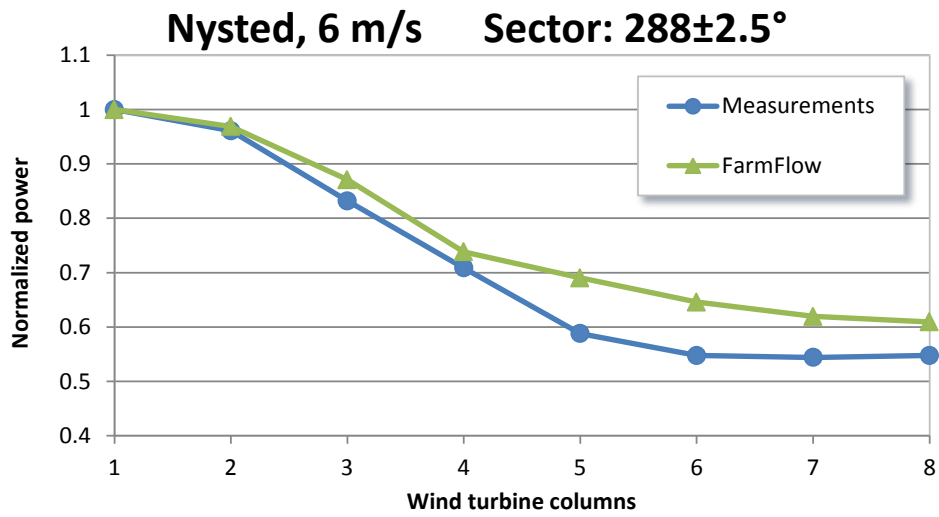
Nysted, 6 m/s   Sector: 293±2.5°
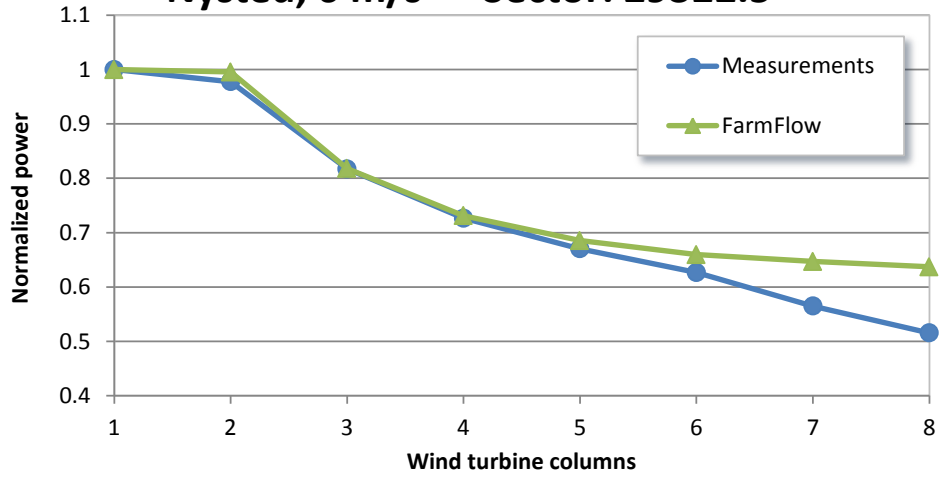
Nysted, 8 m/s   Sector: 293±2.5°

Nysted, 10 m/s   Sector: 293±2.5°